Kinetics of precipitation of non-ideal solid-solutions in a liquid environment

Claudine Noguera, B. Fritz, A. Clement

Kinetics of precipitation of non-ideal solid-solutions in a liquid environment.

C. Noguera,[1] B. Fritz,[2] and A. Clément[2]

[1] *CNRS-Sorbonne Universités, UPMC Univ. Paris 06, UMR 7588, INSP, F-75005 Paris, France*
[2] *Université de Strasbourg/EOST,CNRS, Laboratoire d'Hydrologie et de Géochimie de Strasbourg, 1 rue Blessig, F-67084 Strasbourg Cedex, France*

(Dated: April 1, 2016)

We present a theoretical formalism which, for the first time, accounts for the nucleation, growth and/or redissolution of binary non-ideal solid-solutions, whether mineral or bimetallic, in solution. It yields the time evolution of all ion activities, together with the particle population characteristics: number, size and composition profile of particles as a function of time and of their time of nucleation. It is shown that depending on the Guggenheim parameter values which drive the non-ideality of the solid-solution, on the ratio of the solubility products of the end-members and on initial conditions, different scenarios of precipitation may take place, in which particles display composition profiles which may be smooth or discontinuous. An illustration of the characteristics of precipitation in the various scenarios is given, by simulations performed under some simplifying assumptions and qualitative predictions are made for the precipitation of some mineral solid solutions of geochemical interest. To our knowledge, this is the first time, in the fields of both geochemistry and metallic alloys, that these out-of-equilibrium precipitation processes of non-ideal solid-solutions are fully described.

Highlights:

- Theoretical and numerical model for out-of-equilibrium precipitation of non-ideal solid solutions in a liquid medium.
- For the first time, nucleation, growth and/or redissolution processes are fully described.
- Particle size distribution functions and composition profiles are obtained.
- The formalism applies to mineral $A_{1-x}B_xC$ as well as bimetallic $A_{1-x}B_x$ nanoparticle formation.
- Four scenarios are highlighted; predictions for the precipitation of mineral solid solutions of geochemical interest are made.

Keywords: nucleation and growth, non-ideal solid solutions, miscibility gap, clay minerals, bimetallic nanoparticles, alloy nanoparticles, core-shell nanoparticles, wet-chemical synthesis, kinetic simulation, Nanokin code.

PACS numbers:

I. INTRODUCTION

In natural water-rock interaction systems on the Earth surface, primary minerals are often in a thermodynamic nonequilibrium state. This is the key-condition for the alteration which takes place in the water cycle, including both weathering processes near surface and hydrothermal alteration at depth. The resulting spontaneous dissolution of primary minerals leads to the formation of secondary minerals which are generally not defined compounds but often solid solution phases (SS), with compositions that adjust to the evolution of the chemical composition of the aqueous solution (AS). The most frequent example of this property is the formation of clay mineral phases in the alteration of rock-forming silicates (Millot, 1970; Meunier and Velde, 1989), but many oxides, carbonates, and sulfates also share this property (Drever, 1984; Geiger, 2001; Rhada and Navrotsky, 2013).

In another context, formation of bimetallic nanoparticles is often the aim of wet chemistry experiments in the laboratory, due to their interesting properties for plasmonics (Major et al., 2009), catalysis (Zhang et al., 2011) or electrocatalysis (Peng and Yang, 2009) applications. Similarly to their mineral counterparts, these alloys may display an ideal SS behavior, or, alternatively, a tendency towards ordering or demixing (phase separation), depending upon the sign and strength of their mixing enthalpy of formation (Ferrando et al., 2008).

The equilibrium behavior of a SS in contact with an AS, whether ideal or non-ideal, is now well established (Lippmann, 1982; Glynn and Reardon, 1990), as reviewed by Ganguly (2001) or Prieto (2009). The relationship between the SS composition and the distribution of ions in the AS may be represented by the classical Lippmann's or Roozeboom's diagrams (Lippmann, 1980; Roozeboom, 1904). Recent theoretical studies of non-ideal mineral SSs at equilibrium mainly concern cements and concretes interacting with the AS, particularly in the field of nuclear waste storages and clay barriers (Börjesson et al., 1997; Walker et al., 2007) but carbonate SSs have also been considered (Kulik et al., 2010; Katsikopoulos et al., 2009).

As far as the kinetics of SS formation are concerned, experiments making use of counter-diffusion of reactants

through a porous medium (Prieto et al., 1997; Sánchez-Pastor et al., 2006) or in situ atomic force microscopy studies of the growth of SSs in a fluid cell (Pina et al., 2000; Putnis et al., 2002; Astilleros et al., 2003; Astilleros et al., 2006) have provided important information on growth mechanisms and particle composition for various mineral SSs.

Inclusion of kinetic effects in the modeling of a SS formation still remains a difficult task. In the water-rock interaction model KINDIS (Madé et al., 1994) and its extension for treating reaction and transport (Nourtier-Mazauric et al., 2005), kinetic dissolution and precipitation at equilibrium of ideal SSs were included but without considering nucleation and growth. In these works, a single SS was allowed to precipitate for a given set of end-members, corresponding to the least soluble phase or, equivalently, to the phase with the highest supersaturation. More recent approaches rely on empirical rate equations, not considering explicitly nucleation, size-dependent growth and nucleation (Shtukenberg et al., 2010, Brandt et al., 2015). The same was true in the coupled reaction and transport model by Lichtner and Carey (2006) who represented the SS by a discrete set of stoichiometric solids with fixed composition. On the other hand, atomistic Monte Carlo simulations of ideal SSs under constant supersaturation have specified how the distribution coefficients vary with the supersaturation at kink, step and terrace sites of the growing particles (Matsumoto and Kitamura, 2001; Matsumoto et al., 2005). Only in the work of Pina and Putnis (2002) did a generalized expression for the nucleation rate appear, and the composition of the critical nucleus was determined from the maximum of the nucleation frequency. However, growth and feed-back effects were not included in this work.

To our knowledge, only in our previous works (Noguera et al., 2010; Noguera et al., 2012), were the full dynamics of a SS formation fully accounted for, with the inclusion of nucleation processes, size dependent growth, particle population and out-of-equilibrium composition of the critical nuclei and deposited layers during growth. This has led to the creation of a second version of the NANOKIN code (Noguera et al., 2010), which previously could only account for the kinetics of formation of minerals with fixed composition (Fritz et al., 2009). However this second version was restricted to ideal binary SSs.

It is our goal, in the present work, to propose a theoretical description of nucleation and growth of *non-ideal* binary SSs. As will appear clearly in the following, it does not consist in merely introducing activity coefficients in the nucleation and growth equations. Depending on the strength of the enthalpy of mixing, which will be represented by a Guggenheim expansion restricted to two terms (sub-regular SS), and depending on the composition of the AS, several scenarios may take place in which the composition profiles of the formed particles and the precipitation dynamics are distinctly different. Each of these scenarios will be exemplified by a numerical simulation, under some simplifying assumptions and predictions will be made for various mineral SSs of geochemical interest to assess which scenario applies to each of them.

The formalism primarily aims at describing SSs of the $A_{1-x}B_xC$ type, relevant e.g. to mineral SSs with homovalent substitution, like $(Ba,Sr)CO_3$. However the generalization to SSs of the $A_{1-x}B_x$ type, such as bimetallic SSs, is straightforward because it only requires skipping the C activities. In that way, our work can also be useful in the field of metallic alloys in which, to our knowledge, only thermodynamic aspects of the formation of bimetallic nanoparticles in wet chemistry experiments have been considered. We will use the generic term "aqueous" solution to refer to the solution in which precipitation takes place, whether it contains water or not.

The paper is organized as follows. In section II, we introduce thermodynamic concepts which are required for describing binary non-ideal (sub-regular) SSs in contact with an AS. We propose a new representation of the stoichiometric saturation condition, distinct from the Roozeboom diagram. It is more compact than the latter and turns out to be extremely useful in understanding the scenarios of precipitation of strongly non-ideal SSs. In section III, IV and V we present the theoretical background and master equations for nucleation, growth and feed-back effects on the chemical composition of the AS, respectively. Then, in Section VI, we discuss the characteristics of the precipitation process as a function of the degree of non-ideality of the SS and the initial conditions. We highlight four possible scenarios of precipitation and we devise a diagram of their occurrence as a function of the solid and AS characteristics. Finally, we illustrate the characteristics of precipitation in the various scenarios, by simulations performed within some simplifying assumptions, and we make qualitative predictions of the precipitation characteristics of SSs of geochemical interest (Section VII), before concluding. The text is complemented by five appendices in which most of the formal equations are derived.

II. THERMODYNAMIC CONCEPTS

In this section we first recall some useful concepts relevant for a SS in contact with an AS of given composition. This will allow us to introduce quantities, such as the stoichiometric solubility product, the stoichiometric saturation state of the AS with respect to the SS, and the concept of stoichiometric saturation. Then we will discuss in detail how the latter depends on the non-ideality characteristics of the SS, which will be a useful step before addressing out-of-equilibrium processes.

We consider a SS of composition $A_{1-x}B_xC$ ($0 < x < 1$), with AC and BC its end-members. In the following, A, B and C will represent the relevant aqueous species in the AS and [A], [B] and [C] their activities, respectively. The solubility products of the end-members, denoted

K_{AC} and K_{BC}, are functions of the standard changes in Gibbs free energy, ΔG_{AC} and ΔG_{BC}, for dissolution:

$$\begin{aligned} K_{AC} &= \exp\left(-\Delta G_{AC}/RT\right) \\ K_{BC} &= \exp\left(-\Delta G_{BC}/RT\right) \end{aligned} \quad (1)$$

in which R is the gas constant and T the temperature.

Considering the SS as a single component stoichiometric solid, the change of Gibbs free energy $\Delta G(x)$ during the dissolution of one mole of composition x may be written as:

$$\begin{aligned} \Delta G(x) = (1-x)\Delta G_{AC} + x\Delta G_{BC} + \Delta G_M^E(x) \\ -RT\left(x\ln x + (1-x)\ln(1-x)\right) \end{aligned} \quad (2)$$

The sum $(1-x)\Delta G_{AC} + x\Delta G_{BC}$ represents the change of Gibbs free energy for a mechanical mixture of AC and BC. It is complemented by the ideal entropy of mixing (on the second line), assuming full disorder of the A and B species in the SS. $\Delta G_M^E(x)$ is the excess free energy of mixing, which includes the excess entropy of mixing $\Delta S_M^E(x)$ and the enthalpy of mixing $\Delta H_M(x)$: $\Delta G_M^E(x) = \Delta H_M(x) - T\Delta S_M^E(x)$. We will neglect $\Delta S_M^E(x)$ which may originate from non-configurational entropy (Benisek and Dachs, 2012) or deviations from perfect randomness. As regards $\Delta H_M(x)$, whose variations with the SS composition are usually represented by the Guggenheim expansion (Guggenheim, 1937), we will only keep its first two terms, and thus restrict ourselves to sub-regular SS:

$$\Delta H_M(x) = -RTx(1-x)[A_0 + A_1(2x-1)] \quad (3)$$

The two dimensionless parameters A_0 and A_1 characterize the non-ideality of the SS. A_0 may be related to first neighbor pairwise interactions. Its sign drives the tendency to ordering (if negative) or to unmixing (if positive). When A_0 exceeds some critical value, the SS possesses a miscibility gap, which means a range of compositions in which phase separation takes place. The A_1 coefficient introduces an asymmetry of $\Delta G_M^E(x)$ about $x = 1/2$.

The stoichiometric solubility product of the SS: $K(x) = \exp(-\Delta G(x)/RT)$ is equal to:

$$K(x) = K_{AC}^{1-x} K_{BC}^{x} (1-x)^{1-x} x^x e^{x(1-x)[A_0 + A_1(2x-1)]} \quad (4)$$

One can deduce the stoichiometric saturation state $I(x)$ of the AS with respect to a SS of composition x (sometimes called $\beta(x)$ (Prieto et al., 1993)), equal to the ratio between the ionic activity product $Q(x) = [A]^{1-x}[B]^x[C]$ and $K(x)$:

$$I(x) = \left[\frac{I_{AC}}{(1-x)}\right]^{1-x} \left[\frac{I_{BC}}{x}\right]^{x} e^{-x(1-x)[A_0 + A_1(2x-1)]} \quad (5)$$

In this expression, I_{AC} and I_{BC} are the saturation states of the AS with respect to the pure end-members AC and BC, respectively:

$$I_{AC} = \frac{[A][C]}{K_{AC}} \quad ; \quad I_{BC} = \frac{[B][C]}{K_{BC}} \quad (6)$$

$I(x)$ can also be written in terms of the activity coefficients λ_{AC} and λ_{BC} of the end-members:

$$I(x) = \left[\frac{I_{AC}}{(1-x)\lambda_{AC}(x))}\right]^{1-x} \left[\frac{I_{BC}}{x\lambda_{BC}(x)}\right]^{x} \quad (7)$$

The coefficients λ_{AC} and λ_{BC} depend on x and, for a sub-regular SS, are equal to (Glynn, 1991):

$$\begin{aligned} \lambda_{AC}(x) &= e^{x^2[A_0 + A_1(4x-3)]} \\ \lambda_{BC}(x) &= e^{(1-x)^2[A_0 + A_1(4x-1)]} \end{aligned} \quad (8)$$

Thermodynamic equilibrium between the SS and the AS is reached when simultaneously $I(x) = 1$ (equivalent to $\Delta G(x) = -RT\ln Q(x)$), and $I(x)$ is maximum with respect to x. These two conditions determine the composition x_0 of the SS and that of the AS (through the values of I_{AC} and I_{BC}) at thermodynamic equilibrium. They can be recast under the standard form:

$$\begin{aligned} I_{AC} &= (1-x_0)\lambda_{AC}(x_0) \\ I_{BC} &= x_0\lambda_{BC}(x_0) \end{aligned} \quad (9)$$

In the following, we will focus on the characteristics of the *stoichiometric saturation state*, obtained from the single condition that $I(x)$ is maximum with respect to x. Indeed, the goal of our work is to describe the *kinetics* of precipitation and not the thermodynamic equilibrium between an AS and a SS, which is only found at infinite time of the precipitation process. Using the stoichiometric saturation amounts to considering the SS with respect to which the AS is the most supersaturated (Prieto, 2009). Its composition x_{st} is the solution of the implicit equation (Appendix A):

$$\frac{I_{AC}}{\lambda_{AC}(x_{st})(1-x_{st})} = \frac{I_{BC}}{\lambda_{BC}(x_{st})x_{st}} \quad (10)$$

Such a relationship is often graphically represented in a Roozeboom plot (x_{st},[B]/([A]+[B]) (Mullin, 1993). The discussion which follows, based on Equation 10, paves the route to understanding the composition of the critical nuclei which will be the subject of the following section.

As shown in Appendix A, Eq. 10 may have one or three roots, depending on the values of A_0, A_1, and on the composition of the AS. The latter enters in a compact way through the ratio W, which is equal to:

$$W = \frac{I_{BC}}{I_{AC}} = \frac{[B]K_{AC}}{[A]K_{BC}} \quad (11)$$

When Eq. 10 has a single root, x_{st} varies smoothly as a function of W. When there are three roots, two correspond to maxima of $I(x)$ (i.e. minima of $-\ln I(x)$) and one to a minimum (Figure 11 in Appendix A). The composition x_{st} is equal to the root associated with the lowest value of $-\ln I(x)$. In Figure 1 are represented typical variations of the three roots of Eq. 10 as a function of W and of the corresponding three values of $-\ln(I(x)/I_{AC})$

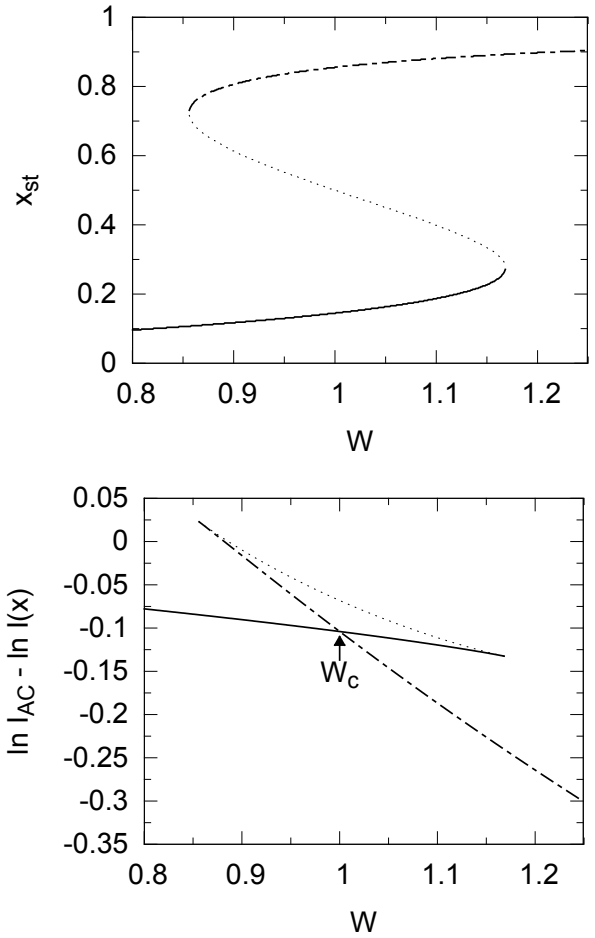

FIG. 1: Top panel: the three roots of Eq. 10, as a function of $W = I_{BC}/I_{AC}$, when $A_0 = 2.5$ and $A_1 = 0$. The full and dashed-dotted curves display the variations of the minima of $-\ln I(x)$ while the dotted one is associated with the maximum of this function. Bottom panel, corresponding values of $\ln I_{AC} - \ln I(x)$. The composition x_{st} of the SS at stoichiometric saturation corresponds to the lowest value of this function. The crossing of the curves at W_c is associated to a discontinuity of x_{st}.

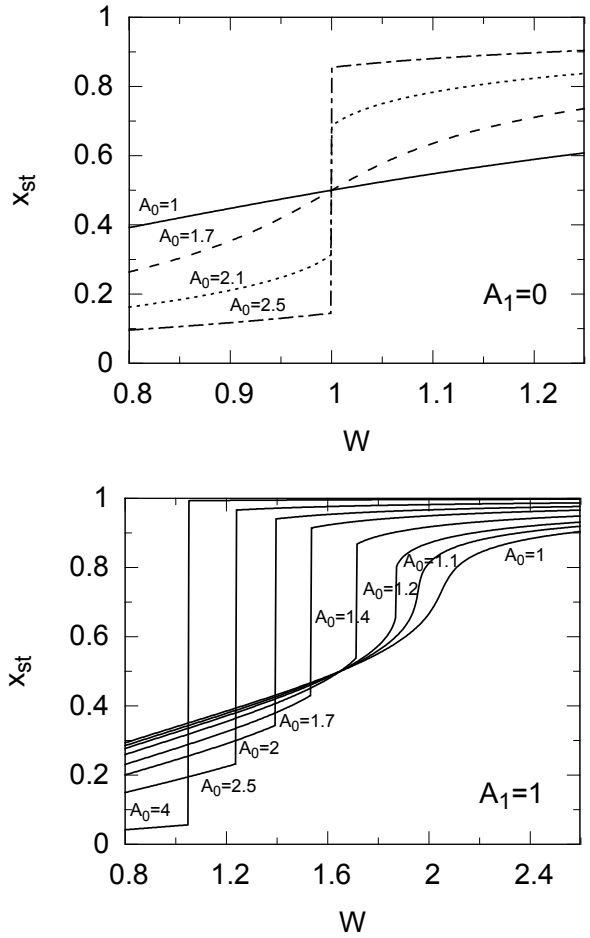

FIG. 2: Composition x_{st} of a SS at stoichiometric saturation with an AS whose composition is characterized by $W = I_{BC}/I_{AC}$, for various values of A_0 when $A_1 = 0$ (top panel) or $A_1 = 1$ (bottom panel).

in the case of a strongly non-ideal SS. Because the latter cross each other, a discontinuity in x_{st} between two values x_1 and x_2 takes place for some AS composition characterized by $W = W_c$, at which the two phases of composition x_1 and x_2 have the same Gibbs free energy per mole. When $W = W_c$, the solid phase may become spatially inhomogeneous and separate into two phases of compositions x_1 and x_2.

Figure 2 shows the variations of x_{st} as a function of W for several values of A_0 and A_1. In the case of regular SSs ($A_1 = 0$), x_{st} varies smoothly (single root in Eq. 10) as long as A_0 remains smaller than 2. x_{st} is less than 0.5 (which means that the SS is richer in A ions than in B ions) whenever $W < 1$ and larger than 0.5 in the opposite case. When A_0 exceeds 2, a discontinuity occurs at $W_c = 1$, whose height increases with A_0 (e.g. $x_2 - x_1 \approx 0.4$ for $A_0 = 2.1$ and 0.7 for $A_0 = 2.5$). The symmetry of the miscibility gap about $x_{st} = 1/2$ is to be linked to the shape of the Gibbs free energy of mixing.

In sub-regular SSs ($A_1 \neq 0$), the transition between smooth and discontinuous variations of x_{st} occurs at smaller values of A_0 and the discontinuity (when it exists) takes place at varying values of W_c. x_1 and x_2 are no longer symmetric about 0.5.

The dependence of W_c on A_0 is represented in Figure 3 (top panel). W_c decreases (resp. increases) asymptotically towards $W_c = 1$, as A_0 becomes larger if $A_1 > 0$ (resp. $A_1 < 0$). On each curve, there exists a minimum value of A_0 below which the discontinuity disappears and x_{st} recovers a smooth variation as a function of the AS composition. The range of parameters $\{A_0, A_1\}$ for which x_{st} has no discontinuity lies inside the region delineated by the two curves drawn in Figure 3 (bottom panel).

Compared to the Roozeboom plot, the representation of x_{st} as a function of $W = ([B]K_{AC})/([A]K_{BC}])$ that we propose presents several advantages. First it acknowledges the fact that, at constant values of the Guggenheim

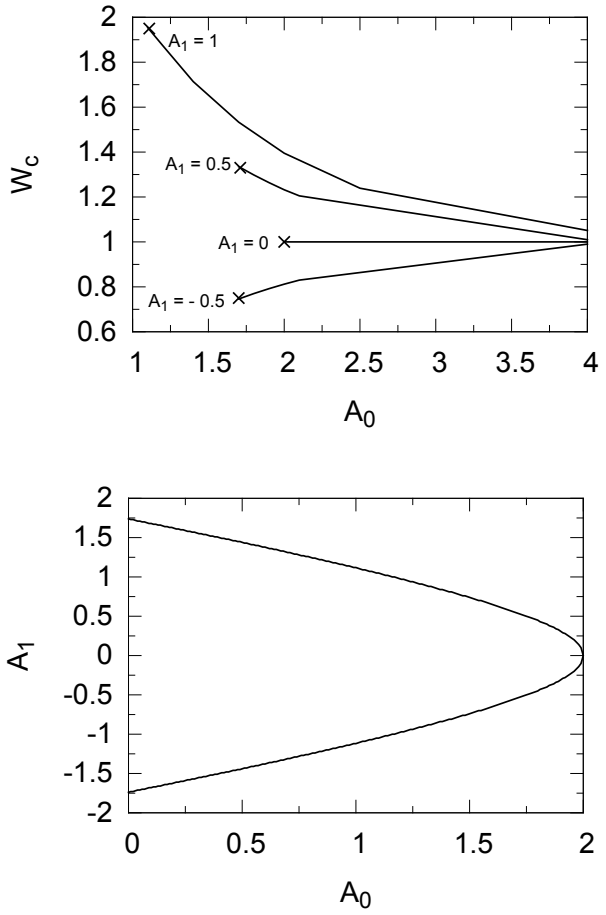

FIG. 3: Top: position W_c of the x_{st} discontinuity as a function of A_0 for A_1=1, 0.5, 0, and -0.5. At constant A_1, the crosses mark the critical A_0 value above which a discontinuity starts taking place. This critical value is represented in the bottom panel as a function of A_1. In the region between the two lines, Eq. 10 has a single root whatever W, which means that x_{st} varies smoothly as a function of the composition of the AS.

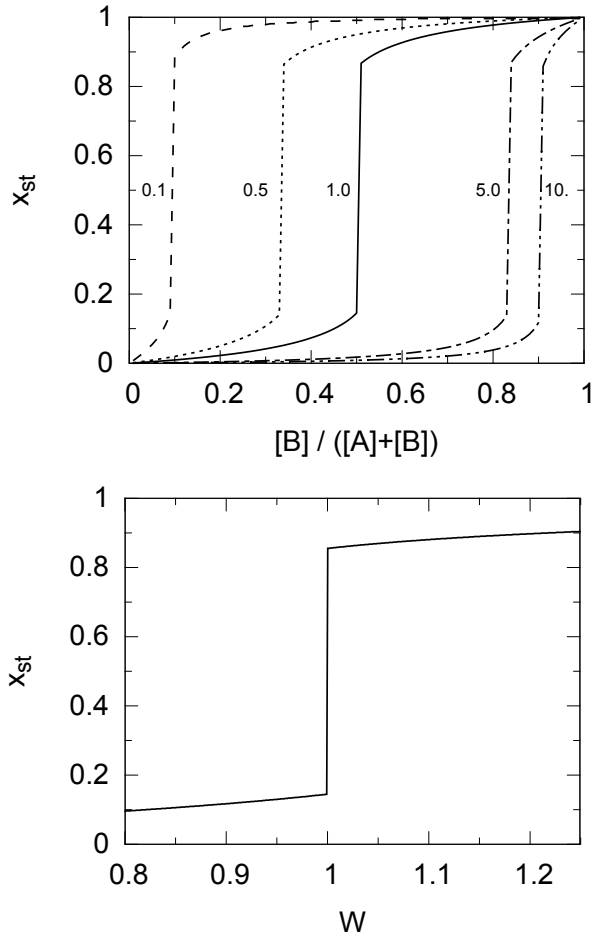

FIG. 4: Two representations of the relationship between the SS composition x_{st} and the AS composition. Top: Roozeboom plot as a function of $[B]/([A]+[B])$ for various values of K_{BC}/K_{AC}. Bottom: Representation as a function of $W = ([B]K_{AC})/([A]K_{BC}])$. In both case the SS is characterized by Guggenheim parameters $A_0 = 2.5$ and $A_1 = 0$.

parameters, x_{st} is uniquely defined by the value of W, and not separately by the ratios $[B]/[A]$ and K_{BC}/K_{AC} as in the Roozeboom representation. The latter, for which one plot is needed for each value of K_{BC}/K_{AC}, is convenient when one considers a specific system. At variance, the representation of x_{st} as a function of W is unique whatever the value of K_{BC}/K_{AC} (Figure 4). It will help highlight the generic behavior of sub-regular SSs during precipitation, which is the goal of our work. As will be shown in the next sections, a representation of the same type will be extremely useful to characterize the composition of the critical nuclei and layers deposited during growth, and to discriminate the various scenarios of precipitation.

III. NUCLEATION

In this section and the two following ones, we extend the formalism of nucleation and growth previously established for the precipitation of minerals with fixed composition (Noguera et al., 2006a,b) and ideal SSs (Noguera et al., 2010) to the formation of non-ideal SSs. Nucleation is treated within the framework of the classical theory of nucleation, in its continuum limit (Markov, 1995;, Adamson, 1960). It is described in the following for homogeneous nucleation of spherical particles. The extension to heterogeneous nucleation (i.e. nucleation of particles on foreign solids) and non-spherical particle shapes is given in Appendix B. Moreover, we send the more complex treatment of precipitation of SSs whose surface energy depends on composition to Appendix C.

Under these conditions (homogeneous nucleation, spherical particles and constant surface energy), the

change in Gibbs free energy $\Delta G(n,x)$ in the formation of a nucleus containing n formula units of composition x is the sum of two terms (k_B the Boltzmann constant):

$$\Delta G(n,x) = -nk_BT\ln I(x) + n^{2/3}v(x)^{2/3}X\sigma \qquad (12)$$

The first (bulk-like) term $-nk_BT\ln I(x)$, with $I(x)$ the stoichiometric saturation state given by Eq. 7, represents the gain (if $I(x) > 1$) of Gibbs free energy when ions from the AS condense into a solid phase. The second term $E_s = n^{2/3}v(x)^{2/3}X\sigma$ is the total surface energy of the nucleus. In this expression, $v(x)$ is the volume of a formula unit of composition x, that will be assumed to vary linearly between its end-member values (no excess molar volume): $v(x) = (1-x)v_{AC}+xv_{BC}$. The geometric factor X is equal to $X = (36\pi)^{1/3}$ for spherical particles and σ is the surface energy per unit area.

When $I(x) > 1$, $\Delta G(n,x)$ displays a maximum as a function of n, which defines the characteristics of the critical nucleus: its size $n_m(x)$ and the barrier to be overcome for its nucleation $\Delta G_m(x) = \Delta G(n_m(x),x)$:

$$n_m(x) = \frac{2u(x)}{\ln^3 I(x)} \quad \text{with } u(x) = \frac{4X^3\sigma^3 v(x)^2}{27(k_BT)^3} \qquad (13)$$

and :

$$\frac{\Delta G_m(x)}{k_BT} = \frac{u(x)}{\ln^2 I(x)} \qquad (14)$$

Assuming that the flow of nuclei through size and composition space is confined to a path through this point only (Reiss and Shugard, 1976), the composition of the critical nuclei is determined by the condition that the nucleation frequency $F(x)$ is maximum with respect to x. $F(x)$ depends exponentially on the nucleation barrier $\Delta G_m(x)$:

$$F(x) = F_0\exp\{-\Delta G_m(x)/k_BT\} \qquad (15)$$

There have been attempts to theoretically estimate the prefactor F_0 for specific systems. However, in most cases, it has resulted in huge (several orders of magnitude) discrepancies with measured values, even in the case of minerals of fixed composition. For this reason, we will assume it to be a constant, with a value that must be empirically determined. The maximum nucleation rate is thus obtained when $\Delta G_m(x)$ is minimum with respect to x, in which case the critical nuclei correspond to a saddle point in the $\Delta G(n,x)$ energy surface.

Taking these expressions into consideration, after some algebra (Appendix D), the minimization of the nucleation barrier yields the critical nucleus composition x^*, solution of the implicit equation:

$$\left(\frac{I_{AC}}{(1-x^*)\lambda_{AC}(x^*)}\right)^{v_{BC}} = \left(\frac{I_{BC}}{x^*\lambda_{BC}(x^*)}\right)^{v_{AC}} \qquad (16)$$

For ideal SSs, Eq. 16 has a single root. For regular or sub-regular SSs, there may be one or three roots and one must determine the one which minimizes the nucleation barrier. To make a link with the previous section, one notes that, except for the exponents v_{AC} and v_{BC}, Eq. 16 strongly resembles Eq. 10, and, indeed, finding its solution(s) amounts to minimizing $-[\ln I(x)]/v(x)$. When $v(x)$ does not depend on x, the composition x^* of the critical nucleus is thus equal to x_{st}, determined previously. When v varies with composition, the minimization of $-[\ln I(x)]/v(x)$ is mathematically more involved (Appendix D). The solutions can be shown to be functions of A_0, A_1, $z = v_{BC}/v_{AC}$ (parameter related to the end-member structures), and of the ratio:

$$W' = \frac{I_{BC}}{I_{AC}^z} \qquad (17)$$

function of the composition of the AS. Depending upon whether the Guggenheim parameter values are located outside or within the region of the miscibility gap, x^* varies smoothly as a function of the AS composition or displays a discontinuity at a value W'_c function of A_0, A_1 and z. Usually z does not differ much from 1, especially for isomorphic end-members, because otherwise there would be no possibility to form an actual SS. As a result, in all cases, the composition x^* of the critical nucleus remains very close to x_{st}. Figure 5, for example, shows how x^* varies with W' for three values of z, in the case of a strongly non-ideal regular SS with $A_0 = 2.5$. The curve associated with $z = 1$ represents the variations of x_{st}. W'_c varies by $\pm 1.6\%$ when $z = 1 \pm 0.15$. The {A$_0$,A$_1$} range, in which a discontinuity of x^* occurs, nearly exactly coïncides with that for x_{st} (Figure 3 bottom panel) within a precision of 0.001 on the limiting values of A_0 and A_1.

Nucleation may start as soon as $I(x^*) > 1$. However, it becomes efficient (more than one nucleus per second and liter of solution), only if $I(x^*)$ exceeds a critical value

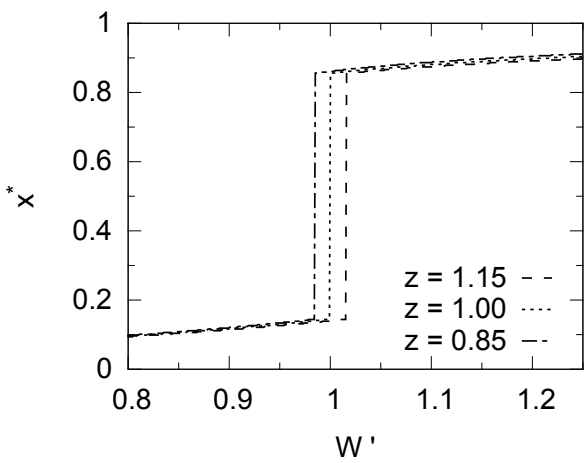

FIG. 5: Composition of the critical nuclei x^*, as a function of the ratio $W' = I_{BC}/I_{AC}^z$, for several values of $z = v_{BC}/v_{AC}$. All curves have been drawn for $A_0 = 2.5$ and $A_1 = 0$. When $z = 1$, $x^* = x_{st}$.

$I_c(x^*)$ defined by:

$$\ln I_c(x^*) = \sqrt{\frac{u(x^*)}{\ln F_0}} \tag{18}$$

All quantities related to a given critical nucleus: x^*, $n^* = n_m(x^*)$, $\Delta G^* = \Delta G_m(x^*)$ and $F(x^*)$, depend on the time t_1 at which nucleation occurs. This time dependence comes from the instantaneous values of the saturation states $I_{AC}(t_1)$ and $I_{BC}(t_1)$ of the AS with respect to the pure SS end-members, entering Eq. 16 which determines $x^*(t_1)$.

IV. GROWTH

Growth involves the condensation of ions from the AS on the surface of the particles. A growth law which correctly describes such processes has to be size-dependent, but its expression depends upon the rate limiting process: diffusion in the liquid or the gaseous phase, continuous interfacial effects, and two-dimensional nucleation on flat faces or spiral growth (Burton et al., 1951; Baronnet, 1982; Parbhakar et al., 1995). In the following, we will restrict ourselves to a continuous growth mechanism, limited by the incorporation of growth units at the surface of a rough nucleus (Markov, 1995; Pina et al., 2000). Furthermore, we will define an average rate of incorporation, so that the particle keeps the same shape as the critical nucleus (Wulff or Wulff-Kaishev shape) during its growth. Actually, the particle size may increase or decrease according to whether it is larger or smaller than the instantaneous size of the critical nuclei. This is the Ostwald ripening process (Ostwald, 1900; Lifschitz and Slyozov, 1961). We will consider the two cases of positive growth or redissolution (negative growth) separately.

A. Positive growth

The energetic cost to increase the dimensions of a particle may be related to its change of volume δV and its change of total surface energy δE_s:

$$\delta\Delta G(x) = -\frac{\delta V}{v(x)} k_B T \ln I(x) + \delta E_s \tag{19}$$

In the following, we will make the assumption of local equilibrium at the particle-solution interface. It amounts to considering that short-range transport across the interface is rapid enough to equilibrate the ions in the liquid and solid layers in contact. It is valid provided that the interface motion is slow enough (Aziz, 1988). When this is the case, the chemical potentials of ions at the surface of the particle are equal to those in the aqueous solution. The composition x of the layer which is deposited is obtained from the condition that $\delta\Delta G(x)$ is minimum with respect to x. The x dependence of $\delta\Delta G(x)$ is included in $-[\ln I(x)]/v(x)$. Determining the composition x of the incremental layer thus amounts to minimizing this quantity. Because it is the same quantity which appears in the determination of the critical nucleus composition, the composition of the incremental layer at time t is thus equal to $x^*(t)$.

Usually, and especially at low temperatures, solid state diffusion is very slow compared to all other characteristic times. We will neglect it, and assume that the composition of a given layer remains fixed once formed (Doerner-Hoskins precipitation (Doerner and Hoskins, 1925)). The particles thus display composition profiles due to the time variation of x^*.

The dimensions and number of growth units of a particle at time t depend on two time indices: t_1 the time at which the particle has nucleated, and t the time of observation. One has thus to write: $n(t_1, t)$ and $\rho(t_1, t)$ (ρ the radius of the particle). At variance, the composition of the outer layer of growing particles only depends on t, because it is the same for all particles.

In the regime of increasing particle size $d\rho(t_1, t)/dt > 0$, the growth equation used for particles of fixed composition can be straightforwardly generalized to SSs (Noguera et al. 2010):

$$\frac{d\rho(t_1,t)}{dt} = \kappa \left(I(t, x^*(t)) - \exp\left[\frac{2u(x^*(t))}{n(t_1,t)}\right]^{1/3} \right) \tag{20}$$

In Eq. 20, it is the saturation index relative to the composition of the deposited layer, and thus relative to a SS of composition $x^*(t)$, which must be used.

B. Redissolution

Whenever the right hand-side of Eq. 20 is negative, i.e. whenever $n(t_1, t) < n^*(t)$, the particles decrease in size ($d\rho(t_1, t)/dt < 0$). During such a redissolution stage, layers formed at anterior times are progressively dissolved. A layer corresponding to a radius $\rho(t_1, t)$ which reaches the particle/solution interface at time t, had been deposited at time t_2 such that:

$$\rho(t_1, t_2) = \rho(t_1, t) \tag{21}$$

t_2 is specific to the particle and thus depends on t_1 and t. At time t_2, the layer composition was equal to $x^*(t_2)$. Consequently, in the redissolution regime, the growth rate reads:

$$\frac{d\rho(t_1,t)}{dt} = \kappa \left(I(t, x^*(t_2)) - \exp\left[\frac{2u(x^*(t_2))}{n(t_1,t)}\right]^{1/3} \right) \tag{22}$$

As a whole, the growth laws written in Eqs. 20 and 22 allow positive or negative growth of particles, depending on the relative value of their size with respect to the critical nucleus size. The process of Ostwald ripening is thus included in the present formalism. At variance, a

growth law of the type:

$$\frac{d\rho(t_1,t)}{dt} = \kappa(I^p(t,x(t_1,t)) - 1)^q \quad (23)$$

as often assumed in the literature (Lasaga, 1984; Parkhust and Appelo, 1999), is unable to lead the solid phase toward equilibrium, whatever the values of the empirical exponents p and q. In the long term, it correctly drives the saturation state of the AS towards 1 if the feed-back effect of growth on the AS composition is included, but because all nucleated particles survive, the total surface energy of the solid phase is not minimized. The lowest energy configuration (a single particle with all available matter in it) is never reached.

V. FEED-BACK EFFECT ON THE SOLUTION

At a given time t, the particle population consists of all the particles which have nucleated at times $t_1 < t$, and with nucleation frequencies and sizes equal to $F(t_1)$ and $n(t_1,t)$ respectively. The amounts $q_M(t)$ of end-members M (M=AC or BC) which have been withdrawn from the AS at time t are thus equal to:

$$q_M(t) = \int_0^t F(t_1)(n^*(t_1)-1)X_M(t_1)dt_1 + \int_0^t F(t_1)dt_1 \int_{t_1}^t dt_3 \frac{dn(t_1,t_3)}{dt_3} X_M(t_3) \quad (24)$$

The first term represents the contribution of nucleation, with $X_M(t_1)$ the molar fractions of the end-members equal to $(1-x^*(t_1))$ and $x^*(t_1)$ for M=AC and BC, respectively. The second term is due to the size evolution of the particles. $n^*(t_1)-1$ is written rather than $n^*(t_1)$ to signal that more than one growth unit is necessary to determine if a solid phase is formed. In the case of redissolution $X_M(t_3)$ must be put equal to $X_M(t_2)$ with t_2 determined by the condition that $\rho(t_1,t_2) = \rho(t_1,t_3)$ (Equation 21). From these quantities and an ionic speciation model, one can calculate all activities in the AS and the saturation indexes $I_{AC}(t)$, $I_{BC}(t)$ and $I(t,x)$.

Including feed-back effects on the AS allows an evolution of its composition towards thermodynamic equilibrium. When $t \to \infty$, $I(t,x^*)$ tends to 1 and, combining Equations 5 and 16, it is easy to check that $x^* \to x_0$, as it should.

The equation giving $q_M(t)$ (Equation 24), together with those which fix $I(t,x)$, $x^*(t_1)$, $n^*(t_1)$, $\Delta G^*(t_1)$, $F(t_1)$, and $\rho(t_1,t)$ form a complete set which, together with the speciation equations, allow the full determination of the precipitate and aqueous solution characteristics at all times.

The present formalism represents an important advance with respect to our previous work (Noguera et al., 2010) which was restricted to ideal solid solutions, spherical particles and homogeneous nucleation. The development of the NANOKIN code to include these new functionalities is presently under progress, and its application to a realistic precipitation process will be the subject of a forthcoming paper. In the following, we will highlight some generic characteristics of the precipitation of non-ideal SS, and, under some approximations, we will present some numerical simulations exemplifying various scenarios which may be encountered in the precipitation of SSs of geochemical interest.

VI. PRECIPITATION SCENARIOS

In this section, we first discuss the characteristics of the precipitation process as a function of the degree of non-ideality of the SS and we evidence four possible precipitation scenarios (Section VI A). We then discuss their conditions of occurrence, under some simplifying assumptions, and we represent them graphically as a function of the ratio of the solubility products of the end-members and the Guggenheim coefficient A_0 (Section VI B).

A. The four scenarios

First we recall that when the Guggenheim coefficients A_0 and A_1 belong to the zone included in between the two lines drawn in Figure 3 (lower panel), the equations which fix x_{st} and x^* have a single root and the precipitation scenario bears strong resemblances to that of an ideal SS. When $A_0 > 0$, the only difference with truly ideal SSs lies in the corrections due to the activity coefficients λ_{AC} and λ_{BC}. In that case the precipitation scenario will be called *Precipitation Scenario #1* (Sc. #1).

When the contribution of the enthalpy of mixing of the SS to the Gibbs free energy of dissolution is negative, the SS displays a tendency towards ordering. It is generally associated with negative values of the first Guggenheim coefficient [1] and is usually interpreted as resulting from short range attraction between dissimilar first neighbors, which favors A-B pairs over A-A or B-B pairs. Which order is actually achieved depends on a contribution of the entropy of mixing which is specific to each case. Because at the present stage our study remains generic, we do not introduce it, so that this limit is not well-treated by our approach and will not be further discussed.

In the limit of strong non-ideality of the SS, a miscibility gap is present which is revealed by a jump of x^* from x_1 to x_2 at a critical value W'_c of $W' = I_{BC}/I^z_{AC}$ (see e.g. Figure 5). This occurs when the Guggenheim coefficients A_0 and A_1 belong to the regions of the diagram in Figure 3 above or below the two lines. x_1, x_2 and W'_c are solely determined by the values of A_0, A_1 and $z = v_{BC}/v_{AC}$ (See Appendix D). For example, in the special case where $A_1 = 0$ (regular SSs) and $z = 1$, x_2 is equal to $1 - x_1$ and the critical value for W is equal to $W'_c = 1$ (see Sections 2 and 3). The question of phase separation in the

[1] For sub-regular SSs, the A_1 coefficient should also be taken into account. However, in the logics of the Guggenheim expansion and its truncation, A_1 is expected to be smaller than A_0, in absolute value, so that extension of the zone of existence of a miscibility gap towards negative A_0 values in Figure 3 appears meaningless.

critical nuclei or in the deposited layers becomes relevant only when $W' = W'_c$ because then the nucleation barrier (Eq. 14) takes equal values for $x^* = x_1$ and $x^* = x_2$ and the same is true for the interfacial Gibbs free energy for growth (Eq. 19).

Consequently, the scenario of precipitation depends on whether and how the condition $W' = W'_c$ is met during the time evolution of the system. The initial conditions (embedded in the value of W' at time $t = 0$) and the sign of dW'/dt in the vicinity of the discontinuity are the relevant factors in that respect. We first note that, in the presence of a miscibility gap, $W'(t)$ has a slope discontinuity at $W' = W'_c$, due to the different values x_1 and x_2 of the SS composition for $W' < W'_c$ and $W' > W'_c$, respectively (Appendix E). We will note dW'_1/dt and dW'_2/dt the associated two time derivative values of $W'(t)$, respectively. This allows discrimination of the following scenarios:

- conditions are such that during the precipitation process the discontinuity is not met. This takes place if, at $t = 0$, $W' < W'_c$ and close to the discontinuity $dW'_1/dt < 0$, or if, at $t = 0$, $W' > W'_c$ and close to the discontinuity $dW'_2/dt > 0$. This scenario will be referred to, in the following, as *Precipitation Scenario #2* (Sc. #2).

- conditions are such that, during the precipitation process, the discontinuity is met but dW'/dt has the same sign on both sides of the discontinuity. The discontinuity is thus crossed but the time spent by the system at $W' = W'_c$ is irrelevant. No phase separation takes place. This scenario will be referred to as *Precipitation Scenario #3* (Sc. #3).

- finally, it may be that the discontinuity is met but dW'/dt has opposite signs on both sides of the discontinuity, which tends to bring it back towards $W' = W'_c$ on both sides. There is then a conflict between the variations of W' forcing it to stay constant and equal to W'_c (Lyapunov stable equilibrium point (Lyapunov, 1992)). It is in this case that phase separation takes place, in order to allow the condition $dW'/dt = 0$ to be fulfilled. This scenario will be referred to as *Precipitation Scenario #4* (Sc. #4).

To go further, one has to determine the sign of dW'/dt on the left and right of the discontinuity. It is possible to derive formal expressions for dW'_1/dt and dW'_2/dt from the feed-back equations, as described in Appendix E, and also to deduce the relative percentages α and $(1 - \alpha)$ of the two SSs with composition x_1 and x_2 when phase separation occurs. These expressions may then be quantitatively estimated for specific cases.

Aside from this numerical approach, in the following, in order to gain some physical insight into practical conditions of occurrence of the four scenarios, we restrict the discussion to regular SSs and some simplified conditions of precipitation. This will allow us to devise a diagram of occurrence of the scenarios as a function of some parameters (ratios of the solubility products of the two end-members, degree A_0 of non-ideality of the SS and initial conditions of precipitation), and to make qualitative predictions of the precipitation characteristics of realistic SSs of geochemical interest.

B. Conditions of existence of the four scenarios for regular SSs

The simplifying assumptions are the following:

- the SS is regular ($A_1 = 0$)

- the formula unit volume as well as the surface energy of the SS are assumed to be independent of x. For example they may be set equal to the average of the corresponding values of the end-members. Consequently, there are no surface excess quantities (Appendix C) and $z = 1$.

- the A, B and C species are the dominant forms of the elements in the AS, and no mineral other than the SS may dissolve or precipitate. The time evolution of the [A], [B] and [C] activities thus only comes from the precipitation of the SS under consideration. Moreover, for SSs with a miscibility gap, we assume that, at the time when the x^* discontinuity is met, redissolution is negligible. Both hypotheses imply that the contribution W" to dW'/dt which is continuous at W'_c vanishes (Appendix E).

Under these hypotheses, in strongly non-ideal SSs ($A_0 > 2$), the miscibility gap is symmetric ($x_2 = 1 - x_1$) and $W'_c = 1$. At the discontinuity, the last equality means that $[B]/[A] = K_{BC}/K_{AC}$. Moreover, close to the discontinuity (Appendix E):

$$\frac{1}{W'}\frac{dW'}{dt} \propto -\left(x^*(t) - (1 - x^*(t))\frac{K_{BC}}{K_{AC}}\right) \qquad (25)$$

with x^* equal to x_1 or x_2 when W'_c is smaller or larger than 1, respectively.

As a consequence:

- $dW'_1/dt > 0$ if $x_1/(1 - x_1) < K_{BC}/K_{AC}$
- $dW'_1/dt < 0$ otherwise
- $dW'_2/dt > 0$ if $x_2/(1 - x_2) < K_{BC}/K_{AC}$
- $dW'_2/dt < 0$ otherwise

Using these inequalities, the conditions of occurrence of Scenario #2 read:

$$\frac{[B(t = 0)]}{[A(t = 0)]} < \frac{K_{BC}}{K_{AC}} < \frac{x_1}{1 - x_1} \qquad (26)$$

or:

$$\frac{x_2}{1-x_2} < \frac{K_{BC}}{K_{AC}} < \frac{[B(t=0)]}{[A(t=0)]} \tag{27}$$

Scenario #3 requires that the three ratios $[B(t=0)]/[A(t=0)]$, $x_1/(1-x_1)$ and $x_2/(1-x_2)$ are simultaneously either smaller than K_{BC}/K_{AC} or larger than it. Finally, Scenario #4 takes place when the following inequalities are fulfilled:

$$\frac{x_1}{1-x_1} < \frac{K_{BC}}{K_{AC}} < \frac{x_2}{1-x_2} \tag{28}$$

whatever the value of [B(t=0)]/[A(t=0)]

These conditions are graphically represented in Figure 6, as a function of $\ln K_{BC}/K_{AC}$ and the degree A_0 of non-ideality of the SS. The boundaries between the zones of existence of the scenarios #1, #2, #3, and #4 include the vertical line $A_0 = 2$ on the left of which only Scenario #1 takes place, and the two lines $\ln K_{BC}/K_{AC} = \ln x_1/(1-x_1)$ and $\ln K_{BC}/K_{AC} = \ln x_2/(1-x_2)$. In between the two latter, phase separation takes place within Scenario #4.

Outside these regions, Scenarios #2 or #3 may take place, depending on the initial conditions. When $\ln K_{BC}/K_{AC} > \ln x_2/(1-x_2)$, the discontinuity is not crossed (Scenario #2) if $[B(t=0)]/[A(t=0)] > K_{BC}/K_{AC}$ and otherwise it is crossed (Scenario #3). Symmetrically, when $\ln K_{BC}/K_{AC} < \ln x_2/(1-x_2)$, the discontinuity is not crossed (Scenario #2) if $[B(t=0)]/[A(t=0)] < K_{BC}/K_{AC}$ and otherwise it is crossed (Scenario #3). The difference between the two scenarios, i.e. the existence of a composition discontinuity inside the particles, is thus only fixed by the initial conditions in these regions.

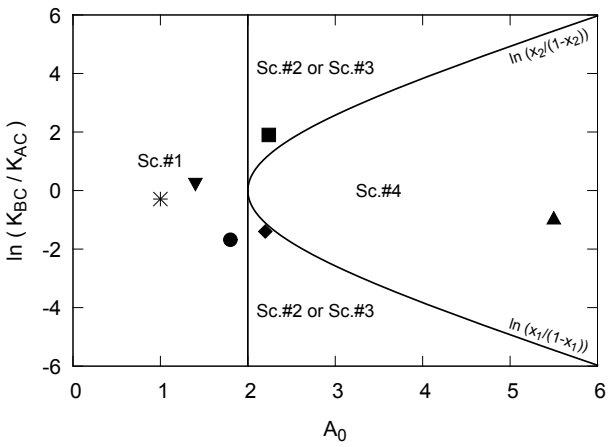

FIG. 6: Diagram $\ln K_{BC}/K_{AC}$ as a function of the degree A_0 of non-ideality of the SS, representing the zones of existence of the scenarios #1, #2, #3, and #4. K(Cl,Br), (Mg,Fe)CO_3, (Ba,Ra)SO_4, (Ca,Zn)CO_3, Ca(SO_4,SeO_4) and (Ca,Sr)CO_3 SSs are located in this diagram, represented by triangle-down, circle, star, diamond, square and triangle-up, respectively (see text).

VII. NUMERICAL SIMULATION AND RELEVANT EXAMPLES

In this section, we present results of numerical simulations which highlight the generic characteristics of the precipitation kinetics under conditions such that scenarios #1, #2, #3 or #4 take place. We will make use of the same assumptions as in subsection VI B and also assume that the particles have a spherical shape. Although these assumptions are rather simplistic, they help provide a first insight into the precipitation characteristics of SSs of geochemical interest.

A. Weakly non-ideal SS: precipitation Scenario #1

When the Guggenheim coefficient $A_0 < 2$, the SS which forms is weakly non-ideal. The only difference from truly ideal SSs lies in the corrections due to the activity coefficients λ_{AC} and λ_{BC}. The dynamics of precipitation presents many common characteristics with that of ideal SSs, which we have analyzed in a previous work (Noguera et al., 2010). Two typical examples are shown in Figure 7, for $A_0 = 1$ and two values of the solubility product ratio K_{BC}/K_{AC}.

In both cases, due to nucleation and growth, the AS is impoverished in A, B, and C species as time passes and $I(t, x^*(t))$ decreases towards 1, until thermodynamic equilibrium is reached in the long term. The time variation of the critical nucleus composition is very dependent on the ratio K_{BC}/K_{AC}. When the solubility products of the two end-members are close to each other, the range of x^* values is small and the composition profile of the particles is smooth, as exemplified in Figure 7 (left panels) where K_{BC}/K_{AC} was chosen equal to 1. At variance, when the two end-members have largely different solubility products, x^* varies in a larger range as shown in Figure 7 (right panels) for which $K_{BC}/K_{AC} = 10$. The surviving particles may display either a core-shell structure, with a smooth interface between core and shell, or nearly constant composition, depending on the initial conditions. In any case, when thermodynamic equilibrium is reached, the last surviving particle has a non-homogeneous composition, at variance with thermodynamic models of SSs which assume an homogenenous composition.

$KCl_{1-x}Br_x$ was shown to be a quasi-regular SS, with $A_0 = 1.4$ and a very small A_1 coefficient (Glynn et al., 1990) and the two end-members have a small solubility product ratio ($K_{BC}/K_{AC} = 1.68$ (Blanc et al., 2012)). The particles formed during precipitation are thus expected to have a smooth composition profile. This is also the case for the (Ba,Ra)SO_4 SS with a ratio of solubility products K_{BC}/K_{AC} equal to 0.512 (Hummel

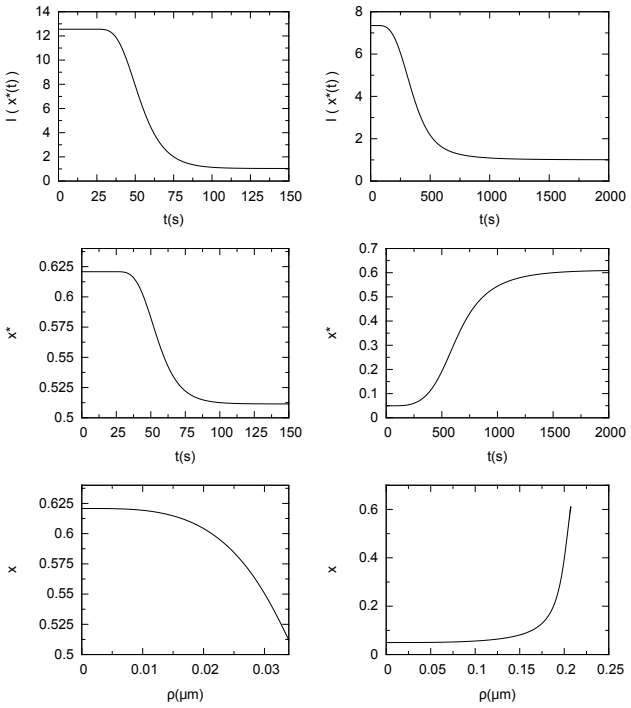

FIG. 7: From top to bottom: time dependence of the saturation state $I(t, x^*(t))$, time dependence of the critical nucleus composition x^* and concentration profile of the surviving particles at the end of the simulation. Left and right panels refer to $K_{BC}/K_{AC} = 1$ and 10, respectively. All curves have been drawn for $A_0 = 1$, $A_1 = 0$, $F_0 = 10^{19}$ particles per second and liter of solution, $\sigma = 50$ mJ/m^2 independent on composition, $\kappa = 10^{-10}$ m/s, $v_{AC} = v_{BC} = 50$ Å^3, $K_{AC} = 10^{-6}$ and initial activities: $[A(t = 0)] = 7.10^{-4}$, $[B(t = 0)] = 9.10^{-4}$, $[C(t = 0)] = 10^{-2}$.

et al., 2002). This SS has recently been studied by Brandt et al. (2015) who confirmed a Guggenheim coefficient $A_0 = 1$ as theoretically predicted (Vinograd et al., 2013). At variance, particles of $Mg_{1-x}Fe_xCO_3$, for which $A_0 = 1.8$ (Chai and Navrotsky, 1996) should display a core-shell structure because the solubility products of the end-members differ by about two orders of magnitude ($K_{BC}/K_{AC} = 0.02$ (Blanc et al., 2012)). The information for the three SSs described above are reported in Figure 6.

B. Strongly non-ideal SS: precipitation Scenario #2 without composition discontinuity

We present here simulation results for the precipitation of a strongly non-ideal SS ($A_0 = 2.5$, $x_1 = 0.1448$ and $x_2 = 0.8552$), under conditions relevant for scenario #2 (Conditions 26 or 27). In Figure 8, initial conditions and ratios of solubility products have been chosen such that $W' < 1$ at $t = 0$ and $dW_1'/dt < 0$. The system thus does not encounter the composition discontinuity and the time dependence of x^* is smooth. The critical

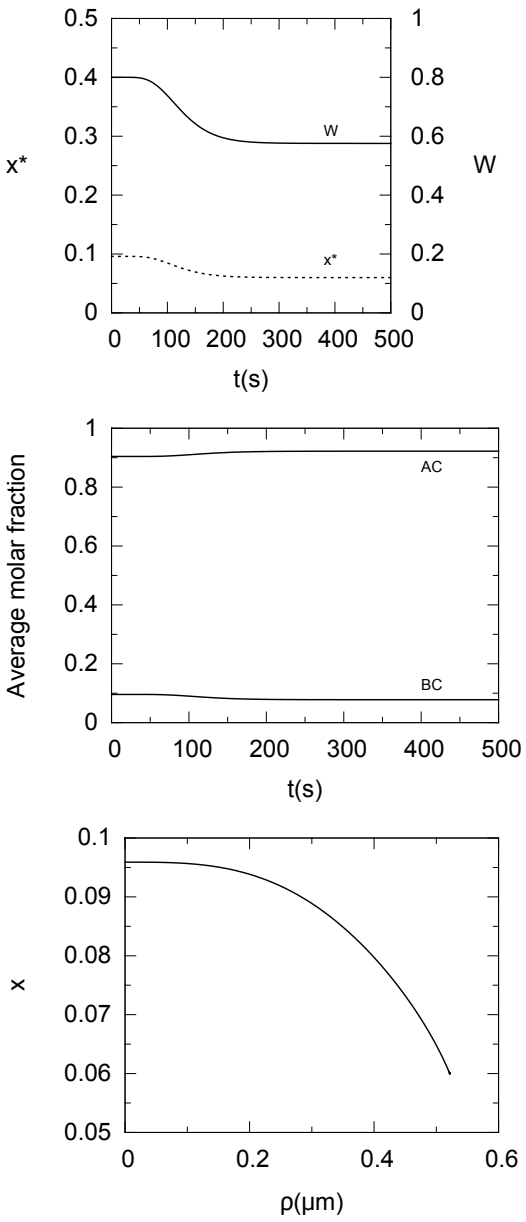

FIG. 8: From top to bottom: time dependence of W and the critical nucleus composition x^*, time dependence of the end-member average molar fractions $q_{AC}/(q_{AC} + q_{BC})$ and $q_{BC}/(q_{AC} + q_{BC})$, and composition profile of long lasting particles. All curves have been drawn for $A_0 = 2.5$, $A_1 = 0$, $F_0 = 10^{19}$ particles per second and liter of solution, $\sigma = 50$ mJ/m^2 independent on composition, $\kappa = 10^{-9}$ m/s, $v_{AC} = v_{BC} = 50$ Å^3, $K_{AC} = 10^{-6}$, $K_{BC} = 10^{-7}$ and initial activities: $[A(t = 0)] = 6.10^{-4}$, $[B(t = 0)] = 48.10^{-6}$, $[C(t = 0)] = 10^{-2}$.

nuclei and the deposited layers remain AC rich during the whole precipitation process, consistent with average molar fractions of the AC and BC end-members in the precipitate, $q_{AC}/(q_{AC}+q_{BC})$ and $q_{BC}/(q_{AC}+q_{BC})$, close to 90% and 10%, respectively. A typical particle composition profile at the end of the process is shown in Figure

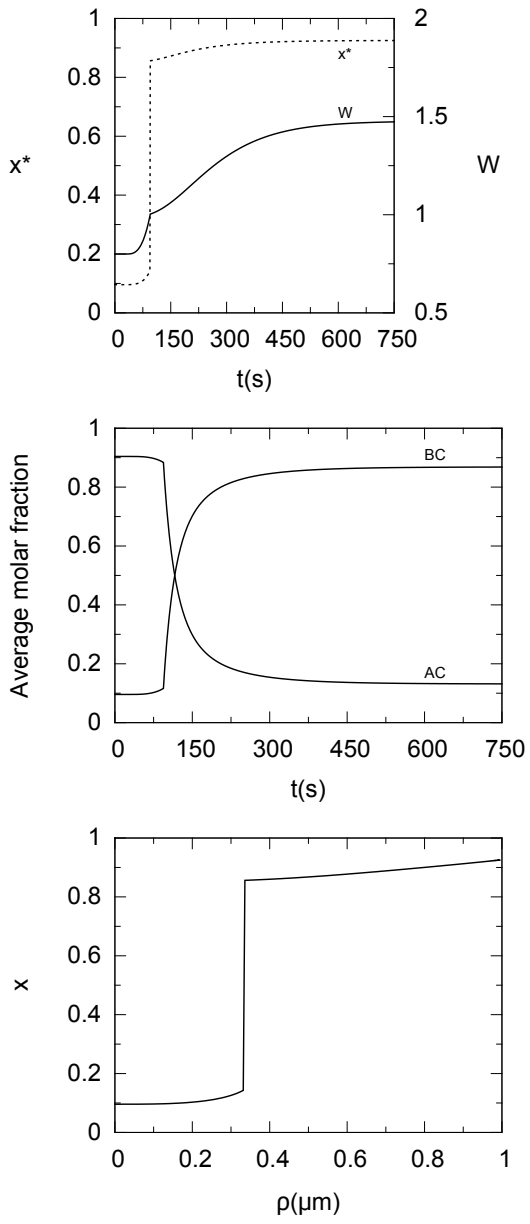

FIG. 9: From top to bottom: time dependence of W and the critical nucleus composition x^*, time dependence of the end-member average molar fractions $q_{AC}/(q_{AC}+q_{BC})$ and $q_{BC}/(q_{AC}+q_{BC})$, and composition profile of long lasting particles. Same parameter values as in Figure 8, except $K_{BC}=10^{-5}$ and $[B(t=0)]=48.10^{-4}$.

8 bottom panel. The particles are non-uniform in composition and become more AC-rich close to their surface. However, the variation of composition x between the core and the surface is small, of the order of 4%.

C. Strongly non-ideal SS: precipitation Scenario #3 with a crossing of the composition discontinuity

This is another example of precipitation of a strongly non-ideal SS, with the same characteristics as the previous one ($A_0=2.5$, $x_1=0.1448$ and $x_2=0.8552$), but under conditions relevant for scenario #3, i.e. such that the discontinuity in the x^* versus W' curve is met and crossed (same sign of dW'/dt on both sides of the discontinuity).

The precipitation characteristics shown in Figure 9 have been obtained under conditions close to those of the previous subsection, except for the initial activity $[B(t=0)]$ and for the ratio of solubility products. At $t=0$, $W'<1$ and $dW'_1/dt>0$. The system thus meets the composition discontinuity at the time t_c when $W'=1$. This clearly shows up in the time dependence of x^* which displays a 70% jump, and in the slope discontinuity in the time dependence of W'. Before t_c, the critical nucleus and deposited layer compositions are AC rich ($x\approx 15\%$). They become BC rich ($x\approx 85\%$) after t_c. This sudden change is reflected in the time dependence of the molar fractions of the end-members in the precipitate which displays a crossing point at some time posterior to t_c. The composition profile of the particles at the end of the process also reflects the discontinuity which has occurred at t_c. The particles have a core-shell structure, with an AC-rich core and a BC-rich shell and an abrupt interface between core and shell (Figure 9, bottom panel).

$Ca_{1-x}Zn_xCO_3$ and $Ca(SO_4)_{1-x}(SeO_4)_x$ SSs may display precipitation scenarios #2 or #3 depending on the initial value of the [Zn]/[Ca] or $[SeO_4]/[SO_4]$ activity ratios. Indeed, for both SSs, the Guggenheim coefficients A_0 are equal to 2.2 (Glynn and Reardon, 1990) and 2.24 (Fernández-González et al., 2006), respectively, and their solubility products locate them, respectively, in the lower and upper regions of Figure 6 where scenarios #2 or #3 take place. ($K_{BC}/K_{AC}=0.03$ for $Ca_{1-x}Zn_xCO_3$ (Crocket and Winchester, 1966) and $K_{BC}/K_{AC}\approx 80$ for $Ca(SO_4)_{1-x}(SeO_4)_x$ (Parkhurst and Appelo, 1999)). During their formation by precipitation, the particles are thus expected to display smooth profiles or core-shell structure depending on initial conditions which will determine whether scenarios #2 or #3 apply.

D. Strongly non-ideal SS: precipitation Scenario #4 with phase separation

Keeping the characteristics of the SS unchanged with respect to the two previous subsections ($A_0=2.5$, $x_1=0.1448$ and $x_2=0.8552$), we now consider conditions relevant for scenario #4, i.e. such that the discontinuity is met but dW'/dt has opposite signs on both sides of the discontinuity. This happens if, at $t=0$, $W'<1$ and close to the discontinuity $dW'_1/dt>0$ and $dW'_2/dt<0$, or if, at $t=0$, $W'>1$ and close to the discontinuity

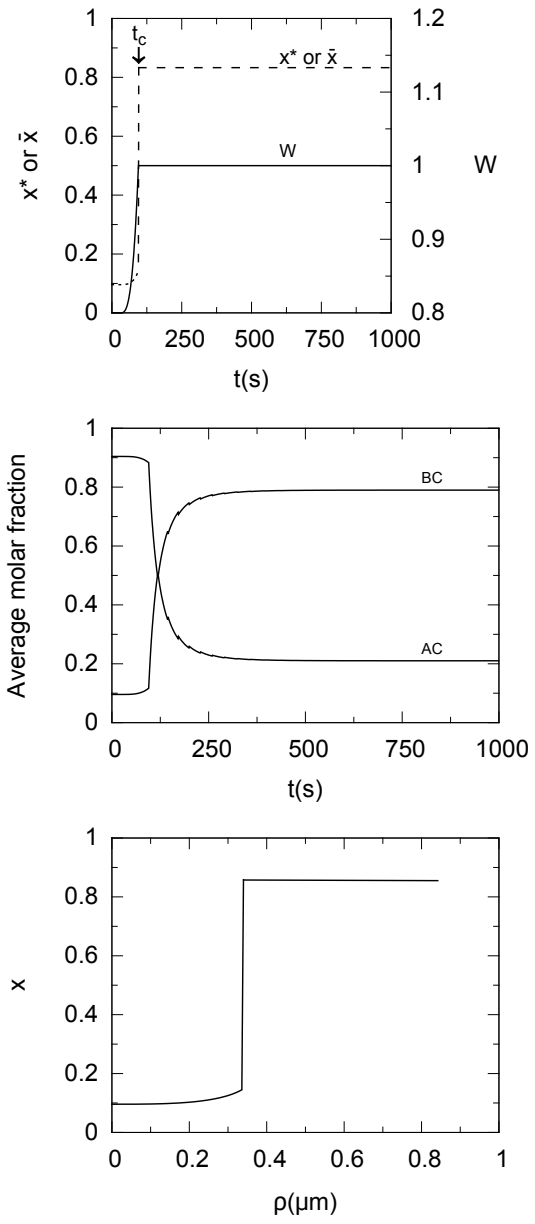

FIG. 10: From top to bottom: time dependence of W, time dependence of the critical nucleus composition x^* (when $t < t_c$) or $\overline{x} = \alpha x_1 + (1-\alpha)x_2$ (when $t > t_c$); time dependence of the end-member average molar fractions $q_{AC}/(q_{AC}+q_{BC})$ and $q_{BC}/(q_{AC}+q_{BC})$; composition profile of a long lasting particle. Same parameter values as in Figure 8, except $K_{BC} = 5.10^{-6}$ and $[B(t=0)] = 24.10^{-4}$.

$dW_1'/dt < 0$ and $dW_2'/dt > 0$ (Condition 28).

For the example shown in Figure 10, initial conditions and ratios of solubility products have been chosen so that $W' < 1$ at $t = 0$, and simultaneously $dW_1'/dt > 0$ and $dW_2'/dt < 0$ at the discontinuity. All other parameters are equal to those of the preceding examples. The system encounters the composition discontinuity at a time t_c. The conflicting variations of W' on the left and right of the discontinuity force W' to remain constant and equal to 1 at all posterior times (Figure 10, top panel). For all times $t > t_c$, the ratio of B and A activities remains constant ($[B(t)]/[A(t)] = K_{BC}/K_{AC}$), although the saturation states I_{AC} and I_{BC} of the AS with respect to the end-members decrease. Phase separation between phases of compositions x_1 and x_2 takes place at $t > t_c$, with relative amounts α and $1-\alpha$ (Eq. 61 in Appendix E). It is not easy to tell how the two phases will be spatially organized, but an average composition in the critical nucleus or the instantaneous deposited layers may be defined at each time $t > t_c$ as $\overline{x} = \alpha x_1 + (1-\alpha)x_2$. Because α remains constant, the same is true for $\overline{x}$, which in the present example is equal to 0.833. Because it is closer to x_2 than to x_1, the end-member molar fractions $q_{AC}/(q_{AC}+q_{BC})$ and $q_{BC}/(q_{AC}+q_{BC})$ strongly vary for $t > t_c$ and tend to approximately $1-\alpha$ and α, respectively, in the long term. A typical particle profile is shown in the lowest panel of Figure 10, highlighting a core-shell structure and an abrupt interface between them.

$Ca_{1-x}Sr_xCO_3$ is a strongly non-ideal SS characterized by a Guggenheim coefficient equal to 5.5 (Casey et al., 1996), indicating poor solubility of Sr in aragonite and a miscibility gap occupying most of the phase diagram ($x_1 \approx 0.004$ and $x_2 \approx 0.996$). Whatever the initial conditions of precipitation, a phase separation is expected, as in the example shown in Figure 10.

VIII. CONCLUSION

We have developed a formalism which describes the precipitation kinetics of non-ideal SSs from an initially supersaturated AS. It treats the time evolution of the AS composition and the formation, growth or redissolution of particles. It extends our previous work, which was restricted to ideal SSs, spherical particles and homogeneous nucleation. The formalism is relevant to both mineral SSs and bimetallic nanoparticle formation. To our knowledge, it is the first time, in the fields of both geochemistry and metallic alloys, that these out-of-equilibrium processes are fully taken into account for non-ideal SSs.

This work highlights how particle composition and size vary with time, resulting in composition profiles which may be smooth or discontinuous, depending on the Guggenheim parameter values which drive the non-ideality of the SSs, and the ratio of the solubility products of the end-members. We have shown that even for strongly non-ideal SSs, phase separation is not the general case and that other scenarios may take place. We have specified their characteristics and under which conditions they may be encountered. Numerical simulations have been performed to exemplify them for a regular SS, under a few simplifying assumptions, and qualitative predictions of the precipitation characteristics of some mineral SSs have been made.

The development of the NANOKIN code to include these new functionalities is presently under progress, and its application to a realistic precipitation process will be

the subject of a forthcoming paper. In the context of water-rock interactions, our work provides enhanced possibilities for analyzing precipitation processes for various SS types, such as carbonates, sulfates or clay minerals, among others.

Appendix A: Condition of stoichiometric saturation

In this appendix, we analyze the mathematical properties of the function $-\ln I(x) = \ln K(x) - \ln Q(x)$ whose minimum determines the stoichiometric saturation condition (Eq. 10 in the text). $-\ln I(x)$ reads:

$$\begin{aligned} -\ln I(x) = &-(1-x)\ln I_{AC} - x\ln I_{BC} \\ &+x(1-x)[A_0 + A_1(2x-1)] \\ &+x\ln x + (1-x)\ln(1-x) \end{aligned} \quad (29)$$

or:

$$\begin{aligned} -\ln \frac{I(x)}{I_{AC}} = &-x\ln W + x(1-x)[A_0 + A_1(2x-1)] \\ &+x\ln x + (1-x)\ln(1-x) \end{aligned} \quad (30)$$

after introducing the ratio W of the saturation states of the AS with respect to the pure end-members:

$$W = \frac{I_{BC}}{I_{AC}} \quad (31)$$

In the following we analyze the variations of the function $f(x)$ equal to the right hand side of Eq. 30. Its first derivative is:

$$\frac{df(x)}{dx} = \ln\frac{x}{W(1-x)} + A_0(1-2x) - A_1(1-6x+6x^2) \quad (32)$$

and its second derivative is:

$$\frac{d^2f(x)}{dx^2} = -2A_0 + 6A_1(1-2x) + \frac{1}{x} + \frac{1}{1-x} \quad (33)$$

There are regions of the parameter space $\{A_0, A_1\}$ where $d^2f(x)/dx^2 > 0$ whatever x. In that case, $f(x)$ is a convex function, with a single minimum. This happens, for example when $A_1 = 0$ and $A_0 < 2$. Otherwise, $f(x)$ may display one minimum, or two minima and a maximum, depending upon the value of W.

Figure 11 exemplifies this latter case when $A_0 = 2.5$ and $A_1 = 0$. At low or high values of W (typically less than 0.86 or more than 1.14), $f(x)$ has a single minimum at x smaller or larger than 0.5, respectively. For intermediate values of W, $f(x)$ has two minima. The composition x_{st} which corresponds to stoichiometric saturation is the one for which $f(x)$ is the lowest. x_{st} displays a discontinuity between x_1 and x_2 at a critical value $W_c = 1$ for which $f(x_1) = f(x_2)$. This behavior is represented in Figure 1 in the main text.

Similar reasoning for different values of A_0 and A_1 leads to Figure 2, which shows that W_c remains equal to 1 whatever the value of $A_0 > 2$ if $A_1 = 0$, but varies with A_0 when $A_1 \neq 0$.

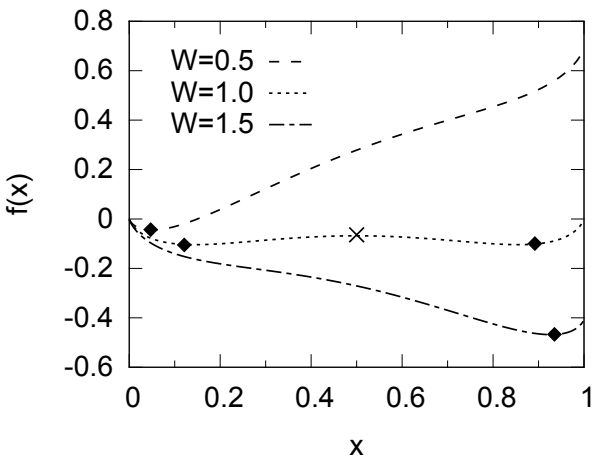

FIG. 11: Curve representative of $f(x)$ (right hand side of Eq. 30) for $A_0 = 2.5$, $A_1 = 0$ and $W = 0.5$, 1. and 1.5. The three curves exemplify the cases when $f(x)$ presents a single minimum at small value of x, two degenerate minima or a single minimum at large x value. The diamonds on the curves mark the positions of the minima and the cross the maximum.

Finally, the limiting values of A_0 and A_1 between regions of discontinuities in x_{st} and regions where it varies smoothly, are obtained from the condition that simultaneously $d^2f(x)/dx^2 = 0$ and, when increasing W, $df(x)/dx = 0$ has, for the first time, three roots. They are represented in Figure 3, bottom panel in the main text.

Appendix B: Precipitation of particles with various shapes

The formalism associated with the homogeneous nucleation and growth of spherical particles has been presented in the main text. However, most solids, except amorphous ones, are non-isotropic and their external shape, which departs from the sphere, reflects the relative energies of their low index faces, as recognized by Wulff (Müller and Kern, 2000 and references therein). Indeed, Wulff theorem states that, at equilibrium, the distance from the center of a particle to its external facets is proportional to the surface energy of these facets. For example, according to Wulff theorem, the aspect ratio of tetragonal particles (basal dimensions $l \times l$ and thickness e, Figure 12), is given by the ratio between the surface energies of the basal and lateral faces (σ_{bas} and σ_{lat}, respectively):

$$\frac{e}{l} = \frac{\sigma_{bas}}{\sigma_{lat}} \quad (34)$$

This result can be extended to the case of particles in equilibrium with a substrate on which they lie on their

basal face. In this case, σ_{bas} is relevant for the face in contact with the AS, and $\sigma_{bas} - W_{adh}$ for the one in contact with the substrate (W_{adh} the adhesion energy). Their aspect ratio is then given by the Wulff-Kaishev theorem:

$$\frac{e}{l} = \frac{\sigma_{bas} - W_{adh}/2}{\sigma_{lat}} \quad (35)$$

If, instead of the basal face, one of the lateral faces is in contact with the substrate, their equilibrium shape involves three inequivalent dimensions l, l' et e. The ratio between these lengths is then equal to:

$$\frac{e}{\sigma_{bas}} = \frac{l}{\sigma_{lat}} = \frac{l'}{\sigma_{lat} - W_{adh}/2} \quad (36)$$

The corresponding expression for rhombohedral particles lying on a substrate on their basal face is:

$$\frac{e}{l} = \sqrt{3}\frac{\sigma_{bas} - W_{adh}/2}{\sigma_{lat}} \quad (37)$$

Similar reasoning can be done for other particle shapes.

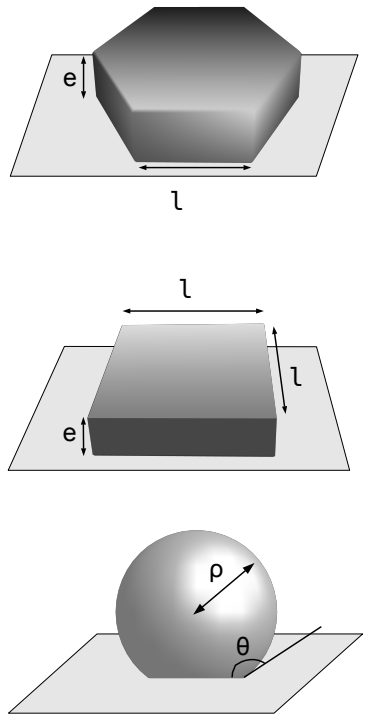

FIG. 12: Representation of rhombohedral, tetragonal and spherical cap particle shapes (from top to bottom).

With these elements in mind, one can consider homogeneous as well as heterogeneous nucleation of particles, assumed to have the Wulff (homogeneous nucleation) or Wulff-Kaishev (heterogeneous nucleation) shapes (Müller and Kern, 2000). The generalized expression of the change in Gibbs free energy for the formation of a critical nucleus then reads:

$$\Delta G(n,x) = -nk_BT \ln I(x) + n^{2/3} v(x)^{2/3} X \overline{\sigma} \quad (38)$$

The geometric factor X and the average surface energy $\overline{\sigma}$ have the following expressions for simple nucleus shapes and for homogeneous or heterogeneous nucleation (Fritz et al., 2009):

- spherical particles:

$$X = (36\pi\Phi(\theta))^{1/3} \ ; \ \overline{\sigma} = \sigma \quad (39)$$

  θ is the wetting angle with the substrate, given by the Young-Dupré equation $-\sigma\cos\theta = \sigma - W_{adh}$, and $\Phi(\theta) = (1-\cos\theta)^2(2+\cos\theta)/4$. For a strong adhesion to the substrate, the wetting angle is equal to 0°, and it is equal to 180° when no wetting occurs (which is also the case for homogeneous nucleation).

- tetragonal particles lying on their basal face:

$$X = 6 \ ; \ \overline{\sigma} = \left(\sigma_{lat}^2(\sigma_{bas} - W_{adh}/2)\right)^{1/3} \quad (40)$$

- tetragonal particles lying on their lateral face:

$$X = 6 \ ; \ \overline{\sigma} = \left(\sigma_{lat}\sigma_{bas}(\sigma_{lat} - W_{adh}/2)\right)^{1/3} \quad (41)$$

- hexagonal particles lying on their basal face:

$$X = 36^{1/3}\sqrt{3} \ ; \ \overline{\sigma} = \left(\sigma_{lat}^2(\sigma_{bas} - W_{adh}/2)\right)^{1/3} \quad (42)$$

To obtain the time evolution of all dimensions during growth, one assumes that the particles keep their equilibrium shape, which allows the use of equations similar to 20 and 22 of the main text for one dimension, deduction of the others from the relationships written above for the ratios between e, l and l', and estimation of the volume V of the particle and finally the number of formula units $n = V/v$.

Appendix C: Precipitation of a SS with composition dependent surface energy

This appendix specifies the modifications to introduce in the formalism which describes SS precipitation when their surface energy depends on composition. The main difference from the simplified treatment, presented in the main text, comes from the existence of surface enrichment effects n_{ACs} and n_{BCs} of AC and BC composition. Starting from a reference state in which the nuclei have a sharp boundary with the aqueous solution (Gibbs dividing surface), such surface excess quantities have to be introduced, so that the Gibbs adsorption equation can be fulfilled (Adamson, 1960; Laaksonen et al., 1999; Noppel et al., 2002; Gaman et al., 2005).

The change in Gibbs free energy $\Delta G(n,x)$ for nucleation now reads:

$$\Delta G(n,x) = -nk_BT\ln I(x) + n^{2/3}v(x)^{2/3}X\overline{\sigma(x)} \\ -n_{BCs}k_BT\ln(\tfrac{I_{BC}}{x\lambda_{BC}(x)}) - n_{ACs}k_BT\ln(\tfrac{I_{AC}}{(1-x)\lambda_{AC}(x)}) \quad (43)$$

The X parameter and the average surface energy $\overline{\sigma}$ have been defined in Appendix B for particles of various shapes. Here $\overline{\sigma}$ is explicitly a function of x. The two last terms in Eq. 43 involve surface excess quantities n_{ACs} and n_{BCs}, multiplied by the corresponding changes in chemical potential $\Delta\mu_{AC}$ and $\Delta\mu_{BC}$. The surface excesses are algebraic quantities, which can take positive as well as negative values.

The expression of the critical nuclei size $n_m(x)$, obtained from the maximum of $\Delta G(n,x)$ with respect to x is the same as in Equation 13. In order to obtain the critical nucleus composition, via the maximum of the nucleation rate, the derivative of $\Delta G_m(x)$ with respect to x has to be performed, with $\Delta G_m(x) = \Delta G(n_m(x),x)$ equal to:

$$\tfrac{\Delta G_m(x)}{k_BT} = \tfrac{u(x)}{\ln^2 I(x)} \\ -n_{BCs}k_BT\ln(\tfrac{I_{BC}}{x\lambda_{BC}(x)}) - n_{ACs}k_BT\ln(\tfrac{I_{AC}}{(1-x)\lambda_{AC}(x)}) \quad (44)$$

and $u(x)$ given in Equation 13. The part which depends on $d\overline{\sigma(x)}/dx$ and the excess quantities n_{ACs} and n_{BCs} vanishes, because it represents the Gibbs adsorption isotherm equation (Adamson, 1960):

$$n(x)^{2/3}v(x)^{2/3}X\frac{d\overline{\sigma(x)}}{dx} = -n_{ACs}\frac{d\Delta\mu_{AC}}{dx} - n_{BCs}\frac{d\Delta\mu_{BC}}{dx} \quad (45)$$

A particularly simple choice for the Gibbs dividing surface is that for which the surface energy does not depend upon the curvature of the surface, in which case the surface excesses fulfill the relationship $n_{ACs}v_{AC} + n_{BCs}v_{BC} = 0$ (Laaksonen et al., 1999). Associated with Eq. 45, it leads to the following values of n_{ACs} and n_{BCs}:

$$n_{ACs}(x) = \tfrac{n(x)^{2/3}Xx(1-x)v_{BC}}{k_BTv(x)^{1/3}[1-2x(1-x)\{A_0+A_1(6x-3)\}]} * \tfrac{d\overline{\sigma(x)}}{dx} \\ n_{BCs}(x) = -\tfrac{n(x)^{2/3}Xx(1-x)v_{AC}}{k_BTv(x)^{1/3}[1-2x(1-x)\{A_0+A_1(6x-3)\}]} * \tfrac{d\overline{\sigma(x)}}{dx} \quad (46)$$

They depend on x and are proportional to the critical nucleus area, while $n(x)$ is proportional to the nucleus volume. They vanish if the surface energy is composition independent. In the absence of detailed information on the x dependence of $\sigma(x)$, a linear law may be assumed between the end-member values of σ.

Excess quantities also contribute to the variation of Gibbs free energy during growth. The energetic cost to change the dimensions of a particle $\delta\Delta G(x)$ reads:

$$\delta\Delta G(x) = -\tfrac{\delta V}{v(x)}k_BT\ln I(x) + \delta E_s \\ -\delta n_{BCs}k_BT\ln(\tfrac{I_{BC}}{x\lambda_{BC}(x)}) \\ -\delta n_{ACs}k_BT\ln(\tfrac{I_{AC}}{(1-x)\lambda_{AC}(x)}) \quad (47)$$

It is related to its change of volume δV, its change of total surface energy δE_s (now a function of x through $\overline{\sigma(x)}$), and its change in excess surface quantities δn_{ACs} and δn_{BCs}. In the minimization of $\delta\Delta G(x)$, the part which depends on $d\overline{\sigma(x)}/dx$ and the excess quantities δn_{ACs} and δn_{BCs} is formally similar to that written for nucleation, and yields similar expressions for δn_{ACs} and δn_{BCs} (Equation 46).

Finally, excess quantities have to be taken into account in the feed-back equations (M=AC or BC):

$$q_M(t) = \int_0^t F(t_1)(n^*(t_1)-1)X_M(t_1)dt_1 \\ + \int_0^t F(t_1)dt_1\int_{t_1}^t dt_3\frac{dn(t_1,t_3)}{dt_3}X_M(t_3) \\ + \int_0^t F(t_1)n_{Ms}(t_1)dt_1 \quad (48)$$

Appendix D: Composition of the critical nuclei

The methodology to determine the composition x^* of the critical nucleus is very similar to that used to find the composition x_{st} of the SS at stoichiometric saturation (Appendix A). Indeed, x^* is obtained from the minimum of the nucleation barrier $\Delta G_m(x)$:

$$\frac{\Delta G_m(x)}{k_BT} = \frac{u(x)}{\ln^2 I(x)} \propto \left(\frac{v(x)}{\ln I(x)}\right)^2 \quad (49)$$

In the right hand side of this equality, we have evidenced the terms which depend on x. Minimizing $\Delta G_m(x)$ with respect to x thus amounts to minimizing $-[\ln I(x)]/v(x)$.

By comparison with Appendix A, it first appears obvious that the composition x^* of the critical nucleus is equal to x_{st} when the formula unit volume $v(x)$ of the SS is independent on x, because then only the minimization of $-\ln I(x)$ must be found. Moreover, we note that the minimum of $-[\ln I(x)]/v(x)$ coincides with that of the function $g(x)$ equal to:

$$g(x) = -\frac{\ln I(x)}{v(x)} + \frac{\ln I_{AC}}{v_{AC}} \quad (50)$$

$g(x)$ can also be written:

$$v(x)g(x) = x\ln x + (1-x)\ln(1-x) \\ +x(1-x)[A_0+A_1(2x-1)] - x\ln W' \quad (51)$$

Aside from the parameters A_0 and A_1, it depends on the ratio $z = v_{BC}/v_{AC}$ of the end-member formula unit

volumes ($v(x) = v_{AC}[1-x+zx]$) and on the composition of the aqueous solution, which enters in a compact way via the ratio $W' = I_{BC}/I_{AC}^z$.

The derivative of $g(x)$ is such that:

$$\frac{v(x)^2}{v_{AC}}\frac{dg(x)}{dx} = \ln x - z\ln(1-x) - \ln W' + A_0\left[(1-x)^2 - zx^2\right] + A_1\left[4x^3(1-z) + 3x^2(z-3) + 6x - 1\right] \quad (52)$$

The terms which depend on A_0 and A_1 turn out to be equal to $\ln\lambda_{BC} - z\ln\lambda_{AC}$, so that equating $dg(x)/dx$ to zero leads to the implicit equation which determines x^* (Equation 16 in the main text):

$$\left(\frac{I_{AC}}{(1-x^*)\lambda_{AC}(x^*)}\right)^{v_{BC}} = \left(\frac{I_{BC}}{x^*\lambda_{BC}(x^*)}\right)^{v_{AC}} \quad (53)$$

The composition x^* of the critical nucleus is thus obtained when simultaneously $dg(x)/d(x) = 0$ and $g(x)$ is minimal. The discussion proceeds along steps similar to those relevant for x_{st}. Depending upon the regions of parameter space $\{A_0, A_1\}$ (which now depends on z), $g(x)$ may be a convex function with a single minimum. Alternatively, it may display one minimum, or two minima and a maximum, depending upon the value of W'. When the latter case occurs, the composition of the critical nuclei is equal to the root x which corresponds to the lowest value of $g(x)$.

Appendix E: Conditions of occurrence of the various scenarios of precipitation

In this appendix, we derive formal relationships allowing the determination of dW'/dt, a crucial quantity to assess which scenario will take place. Moreover, we specify the relative percentage of each phase when phase separation takes place in Scenario #4.

We recast the feed-back equation under the following form:

$$\begin{aligned}\frac{d[A]}{dt} &= -D_0(t)(1-x^*(t)) + D_A(t)\\ \frac{d[B]}{dt} &= -D_0(t)x^*(t) + D_B(t)\\ \frac{d[C]}{dt} &= -D_0(t) + D_C(t)\end{aligned} \quad (54)$$

In these expressions, $D_0(t)$ represents the time derivative of the number of formula units withdrawn from the AS with composition x^*, while $D_A(t)$, $D_B(t)$ and $D_C(t)$ are the variations of A, B and C activities due to either particle redissolution (thus with a surface composition different from $x^*(t)$) or dissolution/precipitation of other minerals present in the AS.

The time derivative $\ln W'$ reads:

$$\frac{1}{W'}\frac{dW'}{dt} = \frac{1}{[B]}\frac{d[B]}{dt} - \frac{z}{[A]}\frac{d[A]}{dt} + \frac{(1-z)}{[C]}\frac{d[C]}{dt} \quad (55)$$

which, after some algebra and using Eq. 54, may be recast under the following form:

$$\frac{1}{W'}\frac{dW'}{dt} = W" - D_0(t)\left(\frac{x^*(t)}{[B]} - \frac{z(1-x^*(t))}{[A]}\right) \quad (56)$$

with:

$$W" = \frac{D_B}{[B]} - \frac{zD_A}{[A]} + \frac{(1-z)D_C}{[C]} - D_0(t)\frac{(1-z)}{[C]} \quad (57)$$

We have separated the contribution $W"$ to dW'/dt which does not present a discontinuity, from the one (second term on the right hand side of Eq. 56) which does present a discontinuity, due to the jump of $x^*(t)$ between x_1 and x_2. In Eqs. 54, 56 and 57, all terms relative to [C] have to be skipped when precipitation of bimetallic $A_{1-x}B_x$ particles is considered.

Whenever Scenario #4 takes place, the cancellation of dW'/dt when $W' = W_c$ yields the relative amounts $D_0(t)\alpha$ and $D_0(t)(1-\alpha)$ of the two SSs with composition x_1 and x_2 when phase separation occurs. From Eq. 56, one obtains:

$$\frac{1}{W'}\frac{dW'}{dt} = 0 = W" - D_0(t)\alpha\left(\frac{x_1}{[B]} - \frac{z(1-x_1)}{[A]}\right) - D_0(t)(1-\alpha)\left(\frac{x_2}{[B]} - \frac{z(1-x_2)}{[A]}\right) \quad (58)$$

and thus:

$$\alpha = \frac{W" - D_0(t)\left(\frac{x_2}{[B]} - \frac{z(1-x_2)}{[A]}\right)}{D_0(t)(x_1-x_2)\left[\frac{1}{[B]} + \frac{z}{[A]}\right]} \quad (59)$$

All these expressions may be easily evaluated numerically to assess which is the scenario relevant for the case under study and, in the case where Scenario #4 applies, Eq. 59 gives the extent of phase separation and its time dependence.

In particular, under the assumptions made in Sections VI B and VII, dW'/dt takes the simplified form:

$$\frac{1}{W'}\frac{dW'}{dt} \propto \left(\frac{x^*(t)}{[B]} - \frac{z(1-x^*(t))}{[A]}\right) \quad (60)$$

which allows the slope discontinuity between $W' < W'_c$ and $W > W'_c$ to be evaluated by replacing x^* by x_1 or x_2, respectively. Moreover, under the same assumptions, when phase separation takes place, the relative percentages α and $(1-\alpha)$ of the two SSs with composition x_1 and x_2 are given by:

$$\alpha = -\frac{\left(x_2 - (1-x_2)\frac{K_{BC}}{K_{AC}}\right)}{(1-2x_2)\left(1 + \frac{K_{BC}}{K_{AC}}\right)} \quad (61)$$

and are independent of time.

IX. REFERENCES

Adamson, A.W., 1960. Physical chemistry of surfaces. Interscience Publishers.

Astilleros, J.M., Pina, C.M., Fernández-Díaz, L., Putnis, A., 2003. Nanoscale growth of solids crystallising from multicomponent aqueous solutions. Surface Science 545, L767-L773.

Astilleros, J.M., Pina, C.M., Fernández-Díaz, L., Prieto, M., Putnis, A., 2006. Nanoscale phenomena during the growth of solid solutions on calcite $10\bar{1}4$ surfaces. Chemical Geology 225, 322-335.

Aziz, M.J., 1988. Non-equilibrium interface kinetics during rapid solidification: theory and experiment. Mater. Sci. Eng. 98, 369-372.

Baronnet, A., 1982. Ostwald ripening in solution. The case of calcite and mica. Estudios Geol. 38, 185-198.

Benisek, A., Dachs, E., 2012. A relationship to estimate the excess entropy of mixing; Application in silicate solid solutions and binary alloys. J. of Alloys and Compounds 527, 127-131.

Blanc, Ph., Lassin, A., Piantone, P., Azaroual, M., Jacquemet, N., Fabbri, A., Gaucher, E.C., 2012. Thermoddem: A geochemical database focused on low temperature water/rock interactions and waste materials. Applied Geochemistry Vol. 27, Issue 10, 2107-2116.

Börjesson, S., Emren, A., Ekberg, C., 1997. A thermodynamic model for the calcium silicate hydrate gel modelled as non-ideal binary sold solutions. Cement and Concrete Research Vol. 27, N° 11, 1649-1657.

Brandt, F., Curti, E., Klinkenberg, M., Rozov, K., Bosbach, D., 2015. Replacement of barite by a $(Ba,Ra)SO_4$ solid solution at close-to-equilibrium conditions: A combined experimental and theoretical study. Geochimica et Cosmochim. Acta 155, 1-15.

Burton, W.K., Cabrera, N., Frank, F., 1951. The growth of crystals and the equilibrium structure of their surfaces. Philos Trans R Soc 243, 299-358.

Casey, W.H., Chai, L., Navrotsky, A., Rock, P.A., 1996. Thermochemistry of mixing strontianite $[SrCO_3(s)]$ and aragonite $[CaCO_3(s)]$ to form $Ca_xSr_{1-x}(CO_3)(s)$ solid solutions. Geochim. Cosmochim. Acta 60, 933-940.

Chai, L., Navrotsky, A., 1996. Synthesis, characterization, and enthalpy of mixing of the (Fe,Mg)CO3 solid solution. Geochim. Cosmochim. Acta 60, 4377-4383.

Crocket, J.H., Winchester, J.W., 1966. Coprecipitation of zinc with calcium carbonate. Geochim. et Cosmochim. Acta. 30, 1093-1109.

Doerner, H.A., Hoskins, W.M., 1925. Coprecipitation of radium and barium sulfates. J. Amer. Chem. Soc. 47, 662-675.

Drever, J.I., 1984. The Chemistry of Weathering. D. Reidel Publishing Co. 324p.

Fernández-González, A., Andara, A., Alía, J.M., Prieto, M., 2006. Miscibility in the $CaSO_4.2H_2O$-$CaSeO_4.2H_2O$ system: Implications for the crystallisation and dehydration behaviour. Chem. Geol. 225, 256-265.

Ferrando, R., Jellinek, J., Johnston, R.L., 2008. Nanoalloys: From Theory to Applications of Alloy Clusters and Nanoparticles. Chem. Rev. 108, 845-910.

Fritz, B., Clément, A., Amal, Y., Noguera, C., 2009. Simulation of the nucleation and growth of simple clay minerals in weathering processes : the NANOKIN Code. Geochim. et Cosmochim. Acta. 73, 1340-1358.

Gaman, A.I., Napari, I., Winkler, P.M., Vehkamäki,, H., Wagner, P.E., Strey, R., Viisanen, Y., Kulmala, M., 2005. Homogeneous nucleation of n-nonane and n-propanol mixtures: A comparison of classical nucleation theory and experiments. J. Chem. Phys. 123, 244502-244512.

Ganguly, J., 2001. in Solid Solutions in Silicate and Oxide systems, Ed. Geiger C. (EMU notes in Mineralogy, Eötvös University Press, Budapest), chapter 3, 37-69.

Geiger, C., 2001. Solid Solutions in Silicate and Oxide systems. (EMU notes in Mineralogy, Eötvös University Press, Budapest).

Glynn P. D., 1991. MBSSAS: a code for the computation of Margules parameters and equilibrium relations in binary solid-solution aqueous solution systems. Computers and Geosciences 17, 907-966.

Glynn, P.D., Reardon, E.J., 1990. Solid-solution aqueous-solution equilibria: Thermodynamic theory and representation. Am. J. Sci. 290, 164-201.

Glynn, P.D., Reardon, E.J., Plummer L. N., Busenberg E., 1990. Reaction paths and equilibrium end-points in solid-solution aqueous-solution systems. Geochim. Cosmochim. Acta 54, 267-282.

Guggenheim, E.A., 1937. Theoretical basis of Raoult's Law. Trans Faraday Soc. 33, 151-159.

Hummel, W., Berner, U., Curti, E., Pearson, F.J. and Thoenen, T., 2002 Nagra/PSI chemical thermodynamic data base 01/01. Nagra Technical Report 02-16.

Katsikopoulos, D., Fernandez-Gonzalez, A., Prieto, M., 2009. Precipitation and mixing properties of the "disordered" (Mn,Ca)CO3 solid solution. Geochim. Cosmochim. Acta 73, 6147-6161.

Kulik, D.A., Vinograd, V.L., Paulsen, N., Winckler, B., 2010. $(Ca,Sr)CO_3$ aqueous solid-solution systems : From atomistic simulations to thermodynamic modelling. Physics and Chemistry of the Earth 35, 217-232.

Laaksonen, A., McGraw,, R., Vehkamäki, H., 1999. Liquid-drop formalism and free-energy surfaces in binary homogeneous nucleation theory. J. Chem. Phys. 111, 2019-2027.

Lasaga, A.C., 1984. Chemical kinetics of water-rock interactions. J. Geophys. Research 86, B6, 4009-4025.

Lichtner, P.C., Carey, J.W., 2006. Incorporating solid solutions in reactive transport equations using a kinetic discrete-composition approach. Geochim. Cosmochim. Acta 70, 1356-1378.

Lifschitz, I.M., Slyozov, V.V., 1961. J. Phys. Chem. Solids 19, 35.

Lippmann, F., 1980. Phase diagrams depicting the aqueous solubility of binary mineral systems. N. Jahrb. Mineral. Abh. 139, 1-25.

Lippmann, F., 1982. Stable and metastable solubility diagrams for the system $CaCO_3$-$MgCO_3$-H_2O at ordinary temperature. Bull. Mineral. 105, 273-279.

Lyapunov, A.M., 1992. The General Problem of the Stability of Motion (A. T. Fuller translation.) Taylor & Francis, London.

Madé, B., Clément, A., Fritz, B., 1994. Modelling mineral/solution interactions : the thermodynamic and kinetic code KINDISP. Comp. Geosci. 20 (9), 1347-163

Major, K.J., De, C., Obare, S.O., 2009. Recent Advances in the Synthesis of Plasmonic Bimetallic Nanoparticles. Plasmonics 4, 61-78.

Markov, I.V., 1995. Crystal growth for Beginners fundamentals of nucleation, crystal growth and epitaxy World Scientific (Singapore, New Jersey, London, Hong Kong).

Matsumoto, N., Kitamura, M., 2001. Effective distribution coefficients of a binary ideal solid solution controlled by kink kinetics. J. of Crystal Growth 222, 667-676.

Matsumoto, K. , Irisawa, T., Kitamura, M., Yokoyama, E., Kumagai, Y., Kouhkitu, A., 2005. Effective distribution of an ideal solid solution crystal : Monte Carlo simulation. J. of Crystal Growth 276, 635-642.

Meunier, A., Velde, B., 1989. Solid solutions in illite/semctite mixed layer minerals and illite. Amer. Mineralogist 74, 1106-1112.

Millot, G., 1970. Geology of Clays. Translated from french. Springer-Verlag, 425p.

Müller, P., Kern, R., 2000. Equilibrium nanoshape changes induced by epitaxila stress (generalized Wulff Kaishef theorem). Surf. Sci. 457, 229-253.

Mullin, J.W., 1993. Crystallization. (Butterworth Heinemann).

Noguera, C., Fritz, B., Clément, A., Baronnet, A., 2006a. Nucleation, growth and ageing in closed systems I : a unified model for precipitation in solution, condensation in vapor phase and crystallization in the melt. J. of Crystal Growth 297, 180-186.

Noguera, C., Fritz, B., Clément, A., Baronnet, A., 2006b. Nucleation, growth and ageing in closed systems II : dynamics of formation of a new phase. J. of Crystal Growth 297, 187-198.

Noguera,, C., Fritz, B., Clément, A., Amal, Y., 2010. Simulation of the nucleation and growth of binary solid solutions in aqueous solutions. Chem Geol. 269, 89-99.

Noguera, C., Fritz, B., Clément, A., 2012. A Theoretical Treatment of the Precipitation of Doubly Substituted Solid Solutions in Aqueous Solutions. Cryst. Growth & Des. 12, 3444-3457.

Noppel, M., Vehkamäkia, H., Kulmala, M., 2002. An improved model for hydrate formation in sulfuric acid-water nucleation. J. Chem. Phys. 116, 218-228.

Nourtier-Mazauric, E., Guy, B., Fritz, B., Brosse, E., Garcia, D., Clément, A., 2005. Modeling the dissolution/precipitation of ideal solid solutions. Oil Gas Sci. Technol. Re. IFP 60, 401-415.

Ostwald, W.Z., 1900. Phys. Chem. Stoechiom. Verwandsch 34, 495.

Parbhakar, K., Lewandowski, J., Dao, L.H., 1995. Simulation model for Ostwald ripening in liquids. J. Colloid Interf. Sci. 174, 142-147.

Parkhurst, D.L., Appelo, C.A.J., 1999. User's guide to PHREEQC (version 2). A computer program for speciation, batch-reaction, one-dimensional transport, and inverse geochemical calculations. US Geological Survey Water-Resources Investigations Report 99-4259 (312 pp.).

Peng, Z., Yang, H., 2009. Designer platinum nanoparticles: Control of shape, composition in alloy, nanostructure and electrocatalytic property. Nano Today 4, 143-164.

Pina, C.M., Enders, M., Putnis, A., 2000. The composition of solid solutions crystallising from aqueous solutions: The influence of supersaturation and growth mechanisms. Chem. Geol. 168, 195-210.

Pina, C.M., Putnis, A., 2002. The kinetics of nucleation of solid solutions from aqueous solutions: A new model for calculating non-equilibrium distribution coefficients. Geochim. et Cosmochim. Acta Vol. 66, No. 2, 185-192.

Prieto, M., Putnis, A., Fernández-Díaz., L., 1993. Crystallization of solid solutions from aqueous solutions in a porous medium: zoning in $(Ba,Sr)SO_4$. Geol. Mag. 130, 289.

Prieto, M., Fernández-Gonzalez, A., Putnis, A., Fernández-Díaz, L., 1997. Nucleation, growth, and zoning phenomena in crystallizing $(Ba,Sr)CO_3$, $Ba(SO_4,CrO_4)$, $(Ba,Sr)SO_4$, and $(Cd,Ca)CO_3$ solid solutions from aqueous solutions. Geochim. et Cosmochim. Acta Vol. 61, No. 16, 3383-3397.

Prieto, M., 2009. Thermodynamics of Solid Solution-Aqueous Solution. In : Thermodynamics and Kinetics of Water-Rock Interaction. Reviews in Mineralogy and Geochemistry vol. 70, 47-85. Mineralogical Society of America and Geochemical Society (Eds).

Putnis, A., Pina, C.M., Astilleros, J.M., Fernández-Díaz, L., Prieto, M., 2002. Nucleation of solid solutions crystallizing from aqueous solutions. Phil. Trans. R. Soc. Lond. A 361, 615-632.

Reiss, H., Shugard, M., 1976. On the composition of nuclei in binary systems. J. Chem. Phys. 65, 5280-5293.

Rhada, A.V., Navrotsky, A., 2013. Thermodynamics of Carbonates, Reviews in Mineralogy and Geochemistry 77, 73-121.

Roozeboom, H.W.B., 1904. Die Heterogenen Gleichgewichte vom Standpunkte der Phasenlehre II. Friedrich Vieweg und Sohn, Braunschweig.

Sánchez-Pastor, N., Pina, C.M., Fernández-Diaz, L., 2006. Relationships between crystal morphology and composition in the $(Ba,Sr)SO_4.H_2O$ solid solution-aqueous solution system. Chem. Geol. 225, 266-277.

Shtukenberg, A.G., Punin, Y.O., Azimov, P.Y., 2010.

Crystallization in Solid Solution-Aqueous Solution Systems: Thermodynamic and Kinetic Approaches. Crystallography Reports Vol. 55, No. 2, 328-341.

Vinograd, V.L., Brandt, F., Rozov, K., Klinkenberg, M., Refson, K., Winkler, B., Bosbach, D., 2013. Solid-aqueous equilibrium in the $BaSO_4$-$RaSO_4$-H_2O system: first principles calculation and a thermodynamic assessment. Geochim. et Cosmochim. Acta 122, 398-417.

Walker, C.S., Savage, D., Tyrer, M., Ragnarsdottir, K.V., 2007. Non-ideal solid solution modeling for synthetic calcium silicate hydrate. Cement and Concrete Research 37, 502-511.

Zhang, H., Okuni, J., Toshima, N., 2011. One-pot synthesis of Ag-Au bimetallic nanoparticles with Au shell and their high catalytic activity for aerobic glucose oxidation. J. Colloïds and Interf. Sci. 354, 131-138.

LIST OF SYMBOLS

Latin characters

A_0, A_1	First and second coefficients of the Guggenheim expansion (dimensionless)
[A]	Activity of the aqueous species A
D_0	Time derivative of the number of formula units withdrawn from the AS with composition x^*
D_A, D_B, D_C	Contributions to the time derivative of [A], [B] or [C] which are continuous at W_c'
E_s	Total surface energy (J)
$F(x)$	Nucleation frequency (number of nuclei/s/liter of solution)
F_0	Prefactor of the nucleation frequency (number of nuclei/s/liter of solution)
ΔG_M	Standard changes in Gibbs free energy for the dissolution of the M end-member (M=AC or BC)
$\Delta G(x)$	Change of Gibbs free energy for a SS of composition x during precipitation or growth
$\Delta G_M^E(x)$	Excess change of Gibbs free energy of mixing for a SS of composition x
$\Delta G(n,x)$	Change in Gibbs free energy for the formation of a nucleus containing n formula units of composition x
$\Delta G_m(x)$	maximum of $\Delta G(n,x)$ with respect to n
$\Delta H_M(x)$	Enthalpy of mixing for a SS of composition x
I_{M}	Saturation state of the AS with respect to the pure end-member M (M=AC or BC)
$I(x)$	Stoichiometric saturation state of the AS with respect to a SS of composition x
$I_c(x^*)$	Critical saturation state of the AS with respect to a SS of composition x
k_B	Boltzmann constant ($1.3806504 \times 10^{-23}$ J/K)
K_{M}	Solubility product of the end-member M (M=AC or BC)
$K(x)$	Stoichiometric solubility product of a SS of composition x
$l(t_1,t)$	Lateral length at time t of a rhomboedral or a tetragonal particle created at time t_1 (m)
$n_m(x)$	Number of growth units in a particle of composition x at the maximum of $\Delta G(n,x)$ with respect to n
$n(t_1,t)$	Number of growth units at time t in a particle created at time t_1
$n_{\mathrm{M}}(x)$	Surface excess quantities of end-member M in a particle
$Q(x)$	Ionic activity product of a SS of composition x
$q_{\mathrm{M}}(t)$	Amount of end-member M withdrawn at time t from the AS (formula unit/liter of solution)
R	Gaz constant (8.314472 J/K/mol)
T	Temperature (K)
x_0	Composition of a SS at thermodynamic equilibrium with an AS
x_{st}	Composition of a SS at stoichiometric saturation with an AS
x^*	Critical nucleus composition
x_1, x_2	Values of the SS composition at the limit of the discontinuity in strongly non-ideal SSs
$\overline{x}$	Mean composition value of the SS when phase separation occurs
v_{M}	Volume of one formula unit of end-member M (m^3)
$v(x)$	Volume of one formula unit of a SS of composition x (m^3)
W	Ratio of the saturation states of the pure end-members $W = I_{BC}/I_{AC}$
W_c	Critical value of W at the composition discontinuity
W'	$W' = I_{BC}/(I_{AC})^z$
W_c'	Critical value of W' at the composition discontinuity
$dW_1'/dt, dW_2'/dt$	Slopes of dW'/dt on the left and right of the discontinuity, respectively
W''	Contribution to dW'/dt which is continuous at W_c'
W_{adh}	Adhesion energy, in the case of heterogeneous nucleation ($\mathrm{J/m}^2$)
X	Geometric factor entering the total surface energy of the particles
z	Ratio of end-members formula unit volumes $z = v_{BC}/v_{AC}$

Greek characters

α	Percentage of the two SSs of composition x_1 and x_2 when phase separation occurs
$\Delta\mu_M$	Change in chemical potential of one formula unit of the M end-member during precipitation (M=AC or BC)
κ	Linear growth constant (m/s)
λ_{M}	Activity coefficient of the end-member M in the SS (M=AC or BC)
$\rho(t_1,t)$	Radius at time t of a spherical particle created at time t_1 (m)
$\overline{\sigma(x)}$	Mean surface energy per unit area of SS particles of composition x ($\mathrm{J/m}^2$)
σ_{lat}, σ_{bas}	Lateral and basal surface energies per unit area of non-spherical particles ($\mathrm{J/m}^2$)
θ	Wetting angle